# Arctic Holocene glacier fluctuations reconstructed from lake sediments at Mitrahalvøya, Spitsbergen

Torgeir O. Røthe [a, c, *], Jostein Bakke [a, c], Kristian Vasskog [b, c], Marthe Gjerde [a, c], William J. D'Andrea [d], Raymond S. Bradley [e]

[a] Department of Earth Science, University of Bergen, Allégaten 41, 5007 Bergen, Norway
[b] Uni Climate, Uni Research, Allégaten 55, 5007 Bergen, Norway
[c] Bjerknes Centre for Climate Research, Allégaten 55, 5007 Bergen, Norway
[d] Lamont-Doherty Earth Observatory of Columbia University, Palisades, NY 10964, USA
[e] Department of Geosciences, University of Massachusetts, Amherst, MA 01003, USA

## ABSTRACT

The Arctic region has experienced a significantly larger warming during the last decades compared to the rest of the world, and model simulations indicate a continued amplification of future global warming in the Polar Regions. A better understanding of natural climate variability in the Arctic is much needed to provide a better context for the observed warming trend. By utilising proxy data it is possible to obtain palaeoclimatic records beyond the range of instrumental observations, which increase our understanding of long-term Arctic climate change. Here, a continuous record of past changes in Equilibrium-Line Altitude (ELA) has been reconstructed for the alpine glacier Karlbreen, located on the northwest coast of Spitsbergen (79° N), based on sediment analyses from a distal glacier-fed lake. A multivariate statistical analysis suggests that the concentration of geochemical elements Ti, Si and K in the lake sediments, together with the physical parameter dry-bulk-density (DBD), reflect changes in the amount of inorganic detrital input to Kløsa, which is closely linked to the size and ELA of the upstream glacier Karlbreen. A linear regression model based on historically documented glacier extents was used to calculate continuous ELA changes back to ~3500 cal. yr. BP. From about 9200 to 3500 cal. yr. BP, the sedimentary record indicates that Karlbreen was very small or had completely melted away. Karlbreen was probably close to its maximum Holocene extent several times during the Neoglacial, first around 1700 cal. yr. BP, then later at ~225 and ~135 cal. yr. BP. An ice-cored moraine system in front of Karlbreen extends well into the main basin of Kløsa, and it is difficult to explain how this moraine could have formed without disturbing the sedimentary record in the lake (e.g. through slumping events). The sedimentary record in Kløsa is continuous and undisturbed over the past 6700 years, suggesting that the outermost moraine formed prior to this time and that it most likely survived the Holocene Thermal Maximum on Svalbard.

© 2014 Elsevier Ltd. All rights reserved.

## 1. Introduction

In recent decades the Arctic region has warmed approximately twice as fast as the global mean, and this "polar amplification" of global temperature rise is expected to continue into the future (Masson-Delmotte et al., 2013). Instrumental climate records are generally sparse in the Arctic and rarely span more than 100 years into the past (AMAP, 2011). Proxy reconstructions are therefore needed in order to study long-term natural climate variability in this region, but few high-resolution terrestrial palaeoclimatic records are currently available. Filling this knowledge gap will enhance our understanding of natural Arctic climate variability, which may in turn shed light on the climate sensitivity of the Arctic.

Glaciers are highly sensitive to perturbations in climate, which makes them excellent indicators of climate change (Oerlemans, 2005), although one should be aware that individual glaciers may respond differently to large-scale climate change due to a range of local factors. In many regions of the world, the largest Holocene

---

* Corresponding author. Department of Earth Science, University of Bergen, Allégaten 41, 5007 Bergen, Norway. Tel.: +47 55 58 81 05.
 E-mail address: torgeir.rothe@geo.uib.no (T.O. Røthe).

glacier extent occurred within the last few hundred years, during the so-called "Little Ice Age" (LIA) (Davis et al., 2009), thereby effectively erasing terrestrial moraine evidence of earlier glacier fluctuations (Bakke and Paasche, 2011). However, lacustrine sediments deposited in distal glacier-fed lakes may be used to reconstruct continuous Holocene glacier fluctuations. Following its introduction by Karlèn (1976), this method has become well-established throughout Scandinavia (Nesje et al., 1991; Dahl and Nesje, 1992; Nesje et al., 2000; Dahl et al., 2003; Lie et al., 2004; Bakke et al., 2005, 2009, 2010; Vasskog et al., 2012). The method links downstream lake sediments to past glacier activity using measurements of physical properties (grain size, density, organic content, water content), geochemical properties (elements analysed at high resolution with XRF scanner), X-ray and magnetic properties (e.g. magnetic susceptibility, ARM, SIRM) along with multiple dating techniques, including radiocarbon dating and $^{210}$Pb dating. Through calibration of the dated sedimentary records with independently dated moraine chronologies or historically documented glacier front positions, it is possible to develop continuous reconstructions of fluctuations in ELA (e.g. Bakke et al., 2010). However, reconstructing glacier fluctuations from distal glacier-fed lakes is particularly challenging in the Arctic due to the logistical difficulties of recovering sedimentary records and because the low amount of organic matter found in Arctic lake sediments makes it difficult to establish robust chronologies using radiocarbon dating (Snyder et al., 1994). Due to these limitations only a few continuous records of past glacier activity based on lake sediments exist from Svalbard (Mangerud and Svendsen, 1990; Svendsen and Mangerud, 1997; Snyder et al., 2000; Mäusbucher et al., 2002).

Here, the first high-resolution and continuous Holocene glacier reconstruction from the northwest coast of the Svalbard Archipelago is presented. Based on a multi-proxy study of sediments recovered from a distal glacier-fed lake the time intervals during which the upstream glacier Karlbreen has been present within the last 9200 years have been determined, and fluctuations in the ELA during the local Neoglacial interval (i.e. the last ~3800 years) have been inferred. The findings indicate that the most distal ice-cored moraine found in front of Karlbreen predates the LIA period and it most likely survived the Holocene Thermal Maximum (HTM) on Svalbard. The results from the sediment analyses together with data from the ground-penetrating-radar (GPR) also allow us to estimate the total erosion rate for a subpolar glacier in the Arctic. The glacier fluctuations correspond to the regional climatic pattern in and around the North Atlantic, as the declining summer insolation seems to be the main driving factor of the past 6000 years.

## 2. Regional setting

### 2.1. Holocene climate- and glaciation history on Svalbard

Following the deglaciation of the area after the Last Glacial Maximum, the glacier coverage was similar or even less compared to the present glacier coverage by 10 100 cal. yr. BP and marks the onset of the HTM on Svalbard (Jessen et al., 2010; Hormes et al., 2013). Several studies have identified a warmer-than-present early Holocene climate on Svalbard, for example as suggested by the presence of blue mussels (Mytilus edulis) along the northern coast, which suggests a summer sea-surface temperature (SST) 1–2 °C warmer than today's (Salvigsen et al., 1992; Salvigsen, 2002). Jessen et al. (2010) report of low concentration of ice-rafted debris from marine sediment cores between 10 000 and 7600 cal. yr. BP at the western coast of Svalbard and suggests few icebergs to be released during this period. A study of macrofossil assemblages in a lake core from Skardtjørna, a lake situated close to Isfjord Radio on the west coast of Svalbard, similarly implies that

summer temperatures were 1–2 °C warmer from ~7000 to ~3000 cal. yr. BP.

About 4000 years ago a gradual cooling in summer temperatures has been inferred based on macrofossil analysis (Birks, 1991). This gradual cooling marks the onset of the Neoglacial period on Svalbard, when glaciers in Linnédalen (southwest Svalbard) showed their initial growth (Svendsen and Mangerud, 1997). Here, frequent glacier expansions have been reconstructed for the Neoglacial period, culminating in the LIA (Werner, 1993; Svendsen and Mangerud, 1997; Lubinski et al., 1999). The late Holocene fluctuations have later been confirmed by $^{10}$Be dating of terminal moraines in front of the Linnébreen (Reusche et al., 2014). $\delta^{18}$O measurements on ice cores from Lomonosovfonna and Holtedahlfonna have been used to reconstruct winter surface-air temperatures for the past 1000 years and indicate gradual winter cooling (approximately 0.9 °C per century) from AD 800 to AD 1800 (Divine et al., 2011). During the 20th century, mass balance measurements and glacier front variations show a general retreat of glaciers on Svalbard (Hagen and Liestøl, 1990; Hagen et al., 1993).

### 2.2. Study area

Mitrahalvøya ("halvøy" = peninsula) is located on the northwest coast of Svalbard (Fig. 1A). A mountain range stretches from south to north on the eastern part of Mitrahalvøya, with summits ranging from 600 to 700 m a.s.l. The study area is located on the northeastern part of Mitrahalvøya, where the alpine glacier Karlbreen ("breen" = Glacier) flows down from Chunfjellet (688 m a.s.l.) towards a series of down-valley lakes.

#### 2.2.1. Catchment area

Meltwater from Karlbreen (79.2397ºN, 11.5358ºE) drains through a chain of lakes ("Inner Moraine Lake", Kløsa, and Erlingvatnet) before reaching the fjord in Signehamna (Fig. 1A). The sediment records presented here are retrieved from Kløsa (~0.25 km$^2$), a 12.5 m deep lake, located downstream from Karlbreen at 42 m a.s.l. Note that the late Weichselian marine limit on the southern tip of Mitrahalvøya is ~20 m a.s.l. (Forman, 1990). The total catchment area of Kløsa is ~3.5 km$^2$, including the "Inner Moraine Lake" (~0.06 km$^2$) and Karlbreen (~1 km$^2$). The relatively low relief of the landscape surrounding Kløsa limits the possibility of large avalanches or debris flows reaching the lake. The short response time needed for paraglacial readjustment in smaller catchments (Ballantyne and Benn, 1994) should also limit the influence of paraglacial processes on the sedimentary budget of Kløsa, particularly towards the middle-to late Holocene. The glacier-lake system studied here should therefore represent an optimal site for reconstructing past glacier fluctuations (Dahl et al., 2003).

Karlbreen has not been classified as a specific glacier type, although small alpine glaciers on Svalbard are usually classified as subpolar (Hagen et al., 1993). A subpolar glacier is characterised by cold-based margins and temperate basal conditions where it is thicker. This classification is based on thermal conditions and may therefore change both temporally and spatially. Glaciers in polar maritime climates may be warm-based in the accumulation zone, and cold-based in the near-surface area of the ablation zone due to winter chilling (Hagen et al., 1993). The occurrence of surging glaciers is widespread on Svalbard and the region have a high number of surge-type glaciers (Hagen et al., 2003; Sund et al., 2014). Smaller cirque glaciers are not typically found to be surging (Werner, 1993), and no surge-history of Karlbreen is reported. Neither is there any geomorphological evidence (e.g., abnormal margins, loop-shaped moraines, etc.) of surge-type behaviour found in relation to Karlbreen.
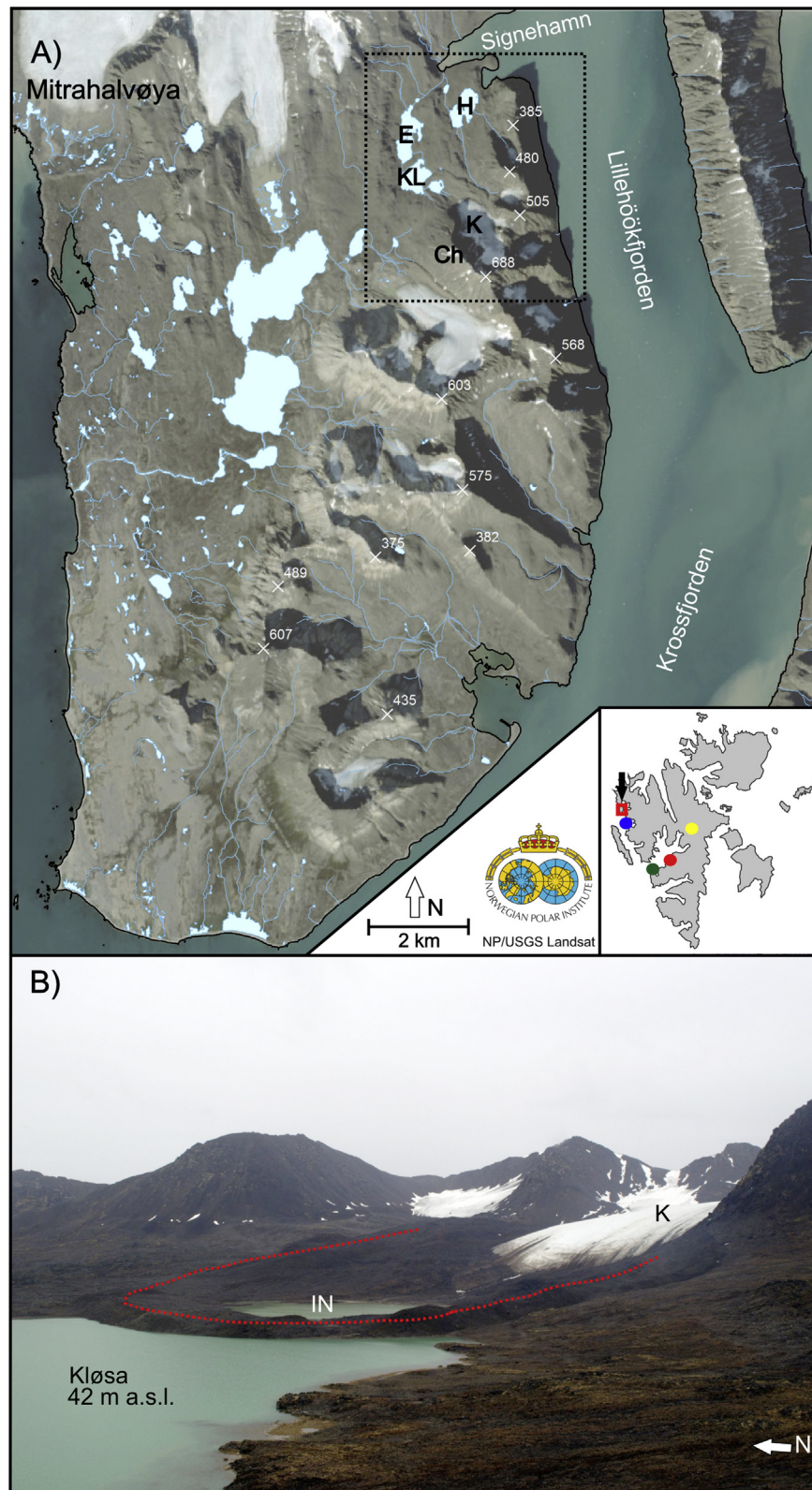
**Fig. 1.** A: Aerial photo of Mitrahalvøya showing the study area (broken lines), the letters refers to: K = Karlbreen, KL = Kløsa, E = Erlingvatnet, H = Hajeren and Ch = Chunfjellet (fjell = mountain). The numbers (in white) on the map corresponds to height above sea level. Inlet map showing Svalbard and the position of the study area by the arrow, coloured dots refer to Ny-Ålesund (blue), Kongressvatnet and Linnévatnet close to Isfjord Radio/Kapp Linné (green), Lomonosovfonna (yellow) and Longyearbyen (red). B: Photo from the study area with a view towards the east. Note the distinct moraine damming "Inner Moraine Lake" (red dotted line). (For interpretation of the references to colour in this figure legend, the reader is referred to the web version of this article.)

A distinct moraine ridge dams the "Inner Moraine Lake" downstream from Karlbreen. It stretches out from the foot of Chunfjellet in the west and forms a distinct lobe-shape that separates Kløsa from the "Inner Moraine Lake" (red dotted line in Fig. 1B). The distal side of the ridge is steep (between 45° and 60° and 12−24 m high along the ridge) compared to the proximal side (between 2° and 10°). The size, shape and position of the moraine ridge is typical for glacier forefields on Svalbard and most likely contains a core of ice (Glasser and Hambrey, 2005).

Moraines of this type are thought to form due to a continuous supply of debris to the glacier margin that increases the debris cover at the glacier snout, thereby causing an insulating effect. In a period of warming the debris will then protect the glacier front from melting while the rest of the glacier retreats, thereby forming a detached ice-cored moraine (Lukas, 2011). Similar moraine ridges are found in front of many glaciers on Svalbard, and the outermost ridges are commonly interpreted to be of LIA origin based on lichenometry dating on the west coast of Svalbard (Werner, 1993).

Metamorphic rocks make up the bedrock lithology in the catchment area of Kløsa, as the study area is located within the Signehamna Formation. Garnet-mica schist dominates the southern part of Chunfjellet, whereas mica schist dominates the rest of Kløsa's catchment (Ohta et al., 2008).

## 2.3. Climate

The climate along the west coast of Svalbard is significantly influenced by the West Spitsbergen Current (WSC), a branch of the North Atlantic Current that transports warm surface water along the west coast and results in a significantly warmer climate compared to locations at similar latitudes (Førland et al., 2010). The average (1961−1990) June, July and August temperature for the west coast of Svalbard (Ny-Ålesund and Isfjord Radio) is 4 °C, and it ranges between −12 and −15 °C during the winter months (January, February, March). The average (1961−1990) precipitation varies from 190 mm to 440 mm on Svalbard and there is a strong precipitation-gradient from the southwest to the northeast (Førland et al., 2010). Uncertainties are generally large for precipitation measurements in the high Arctic, and the actual amount of precipitation on Svalbard may be somewhat underestimated (Førland and Hanssen-Bauer, 2000; Førland et al., 2011).

## 3. Material and methods

### 3.1. Historical ELA reconstructions

There is a close link between climate and a glacier's Equilibrium Line Altitude (ELA), as the annual mass-balance of a glacier is determined mainly by winter precipitation and summer temperature. The altitude where annual accumulation equals annual ablation on a glacier surface is known as the ELA, and the steady-state ELA is defined as the average altitude where the ELA must be located in order for the glacier to sustain its steady-state frontal position. This relationship can furthermore be used to reconstruct past climate, as any fluctuation in the ELA over time can be used as an indicator for a change in climate (Benn and Lehmkuhl, 2000; Benn and Evans, 2010; Bakke and Nesje, 2011).

Reconstruction of former ELAs at Karlbreen was achieved through both the Accumulation Area Ratio method (AAR) (Porter, 1975) and the Area Altitude Balance Ratio method (AABR) (Osmaston, 2005). The AAR method uses the assumption that the ratio between the accumulation area to the total area typically lies in the range from 0.5−0.8 for a valley/cirque glacier in steady-state with the climate (Porter, 1975). As the AABR method also takes the variation in hypsometry (distribution of surface area over altitude)

of the glacier into account (Osmaston, 2005), this method is found to be better suited to estimate Karlbreen's ELA.

We used a dataset of glacier area outlines issued by König et al. (2013) as a basis for cartographic reconstruction of the earlier extent of the glacier, and the area calculations were performed in ArcMap v. 10.1 (See Fig. VI in Supplementary material) based on contour maps issued by the Norwegian Polar Institute. A spreadsheet from Osmaston (2005) was used for calculating the AABR, using a balance ratio of 2.2. This ratio is in agreement with the data available from the Svalbard region (Rea, 2009).

### 3.2. Coring techniques and mapping of the lake

Both lakes were surveyed by ground penetrating radar (GPR) prior to coring, using a GPR from Malå Geoscience with a 50 MHz antenna, to map out the water depth and sedimentary infill in Kløsa. These data were used onsite to determine optimal coring locations, such as a flat lake bottom and well distributed sediments (Dahl et al., 2003). Kløsa was ice-free when the field campaign took place, and the coring was done from a raft using a modified piston corer (Nesje, 1992) equipped with a 110 mm diameter and 6 m long PVC tube. In addition to this an Uwitec gravity corer was used in order to capture the sediment−water interface at the two main coring sites.

### 3.3. Sediment analyses

Analyses of the sediments included measurements of physical, magnetic and geochemical properties. Samples of 1 $cm^3$ were extracted every 2 cm throughout KLP312 ($N = 140$) for loss-on-ignition (LOI) (Dean, 1974; Heiri et al., 2001), water content (WC) (Menounos, 1997), and dry-bulk density (DBD) analyses (Bakke et al., 2005). The analyses were done to estimate the organic content of the sediments (LOI), whereas the WC and DBD together characterises how the material pack or consolidate under different settings (Bakke et al., 2005).

The magnetic properties were investigated by extracting wet bulk samples every 2 cm from KLP312 ($N = 140$) and sampled into cubic plastic boxes (6.4 $cm^3$) for mass specific susceptibility ($\chi$Bulk), anhysteretic remnant magnetism (ARM) and isothermal remanent magnetization (IRM) analysis. The $\chi$Bulk samples were first measured at room temperature (293 K) on a KLY-2 Kappa Bridge, with a sensitivity of $4 \times 10^{-8}$ SI, and then cooled by liquid nitrogen to 77 K and measured again. The magnetic susceptibility of a paramagnetic mineral varies inversely with temperature, and at 77 K the susceptibility values will be ~3.8 times higher than when measured in room temperature (293 K). This implies that values close to 3.8 will be dominated by paramagnetic minerals and the paramagnetic ratio can be used to infer changes in magnetic state of the minerals (Lanci and Lowrie, 1997). ARM was investigated by inducing the samples to a direct current field of 0.1 mT and to an alternating current field of 100 mT (achieved by a 2G magnetizer). IRM was conducted by applying the sample to a field using a solenoid (Sorensen DTS, 175 mT) and a pulse magnetizer, followed by measurements of the IRM on a cryogenic magnetometer (SQUID) or a Digico Spinner at the BPL. Detrital and biogenic sources of magnetite can to some extent be differentiated by the ratio between ARM and SIRM (Paasche et al., 2004).

Variations in geochemical properties along the surface of KLP312 were analysed using a non-destructive X-ray fluorescence (XRF) ITRAX core scanner at the University of Bergen. The results from the XRF scanner are given as kilocounts-per-second (kcps) and must be regarded as semi-quantitative. The XRF surface scans of KLP312 (278 cm) and KLP112 (266 cm) were analysed for elements ranging from aluminium (Al) to uranium (U), and completed at 200 μm resolution using a chromium (Cr) tube (Croudace et al.,

2006). The total length of 59.6 cm for KLD412 was scanned at a resolution of 500 μm using a molybdenum (Mo) tube at the University of Massachusetts, Amherst (UMASS).

### 3.4. Chronology

The top-most sediments (0–6 cm) of KLD312 were subsampled (0.5 cm) in the field, and afterwards prepared at UMASS for $^{210}$Pb dating at Flett Research in Winnipeg, Canada. Material for $^{14}$C dating was subsampled at 1 cm slices at selected intervals throughout the piston cores from Kløsa. The subsamples were sieved at 125 μm, before plant macrofossils were extracted, dried at room temperature, and placed in sterilised and sealed vials. Only fragments of plant macrofossils were found in the selected intervals throughout KLP312 and this made it difficult to identify the macrofossils. Seven samples were sent to the ETH Zurich − D-PHYS − Ion Beam Physics Laboratories in Switzerland for radiocarbon dating using a gas ion source (Ruff et al., 2007). A further eight samples were sent to the Radiocarbon Dating Laboratory at Lund University in Sweden for radiocarbon dating based on accelerator mass spectrometry analyses (Table 2).

The age−depth model was constructed in Clam 2.1, using the statistical software R (Blaauw, 2010). The radiocarbon-dated samples were calibrated using the calibration curve IntCal13.14C with atmospheric data from Reimer et al. (2013). The age-depth model was built using a smooth spline function (smoothing = 0.7) to interpolate the age between the radiocarbon dates, and includes the $^{210}$Pb dates from the top of the core.

### 3.5. Principal component analysis (PCA)

PCA is an ordination technique that can be used to identify patterns of variability in multivariate data sets (Birks, 1987; Syms, 2008). In multi-proxy records from distal glacier-fed lakes it may be useful for sorting out which of the sedimentary parameters are most likely to reflect input of glacially derived sediments (Vasskog et al., 2012; Bakke et al., 2013). PCA was performed on ten different time series from KLP312, including physical (LOI and DBD), magnetic (χBulk293 K), and geochemical parameters (Ti, K, Ca, Si, Rb, Fe and Mn), using the software Canoco for Windows (v. 4.5) (Lepš and Šmilauer, 2003). In Canoco, all parameters were log-transformed and the resulting PCA scores were standardised. Sections of the core reflecting episodic events (as identified in Section 4.2.1) were removed prior to the analysis. This type of multivariate analysis requires that all parameters have the same sampling resolution, and therefore the higher-resolution geochemical data were smoothed using a 2-cm running mean and resampled at the same resolution as the physical parameters (2 cm).

### 3.6. Erosion rates

The GPR survey of Kløsa together with the well-dated sediment core makes it possible to investigate the total erosion rate in the lake catchment by using the modified equation from Burki et al. (2010):

$$e_{tot} = \frac{V_{pro} \times (1 - p)}{t \times A_{catch}}$$

where $e_{tot}$ is total erosion rate (m/yr),

$t$ is time (yr),
$A_{catch}$ is the catchment area (m$^2$),
$V_{pro}$ is the proglacial sediment volume (m$^3$),
$p$ is the porosity.

The value of $(1 - p)$ is found directly by dividing the residual after loss-on-ignition analyses by the standard particle density (2.65 g/cm$^3$). A constant erosion rate throughout the selected period and no loss of sediment from the basin are assumed when applying this method (Burki et al., 2010). By calculating erosion rates for periods with and without a glacier in the lake catchment, it is possible to estimate an approximate sub-glacial erosion rate for Karlbreen.

## 4. Results

Three piston cores were retrieved from Kløsa during a field campaign in August 2012 (Table 1). Two of the cores, KLP112 and KLP312, were successfully retrieved (Fig. 2), whereas the third core (KLP212) became severely disturbed during coring. KLP312 and KLP112 were retrieved ~150 m apart from each other, and the main sedimentary units were matched between them using titanium (Ti) count rates (see XRF section below) and a visual logging of colour (Fig. 2). KLP112 was slightly disturbed when the core was split and KLP312 was therefore selected as the master core from Kløsa. A comparison with KLD412 (gravity core) suggests that the KLP312 piston core may be lacking the uppermost 1−2 cm of sediment (see Fig. II in Supplementary material), which was likely lost during piston coring.

Core KLP312 was subdivided into seven units (from A to G) based on the lithostratigraphy (visual logging) and XRF measurements of titanium (Ti) (Fig. 2). Below, lithostratigraphic, physical, magnetic and geochemical properties in the KLP312 core are presented (see Figs. 3 and 4). Some of the geochemical elements measured with the ITRAX scanner were rejected due to low countrates and low signal-to-noise ratio and therefore we report only the following elements: silicon (Si), potassium (K), calcium (Ca), titanium (Ti), manganese (Mn), iron (Fe) and rubidium (Rb).

### 4.1. Core stratigraphy KLP312

The bottom part of KLP312, unit G (21 cm), consists of dense sediments with an olive grey colour, which turn to brown 5 cm upwards in the core. In the lower part, the χBulk293 K and DBD values drop from 130 to 70 ($^*10^{-8}$ m$^3$/kg) and from 1.6 to 0.4 g/cm$^3$, respectively (Fig. 3). An opposite pattern is seen in the LOI (from 2 to 11%) and WC values (from 50 to 250%). An undulating sharp boundary at 256 cm marks the transition into unit F. Results from the high resolution elemental analysis (Fig. 4) show an initial drop in XRF count rates at the base of KLP312 for the elements Si, Ti, and K, followed by increasing count rates up towards the undulating border (unit F).

Unit F (68 cm) shows a fining upwards sequence from gravel-sized particles within the sand-sized sediments in the base (256 cm) to clayey sediments at the top (190 cm). The highest count rates in the entire core are found for some of the geochemical elements (Ti, Si and K) in this unit. A sharp drop

**Table 1**
Overview of sediment cores from Kløsa and "Inner Moraine Lake".

| Core | Core location | Length (cm) | Water depth (m) | Coring equipment |
|------|--------------|-------------|------------------|------------------|
| KLD312 | 79.249283°N 11.477067°E | – | 11.5 | "Uwitec Corer" |
| KLD412 | 79.249283°N 11.477067°E | 59.6 | 11.5 | "Uwitec Corer" |
| KLP112 | 79.24596°N 11.47653°E | 266 | 12 | "Nesje Corer" |
| KLP212 | 79.24821°N 11.47155°E | 85 | 8 | "Nesje Corer" |
| KLP312 | 79.24928°N 11.47707°E | 278 | 11.5 | "Nesje Corer" |
| ULP112 | 79.24620°N 11.49035°E | 26 | 5 | "Nesje Corer" |
| ULP212 | 79.24598°N 11.49439°E | 36 | 5 | "Nesje Corer" |

A



B
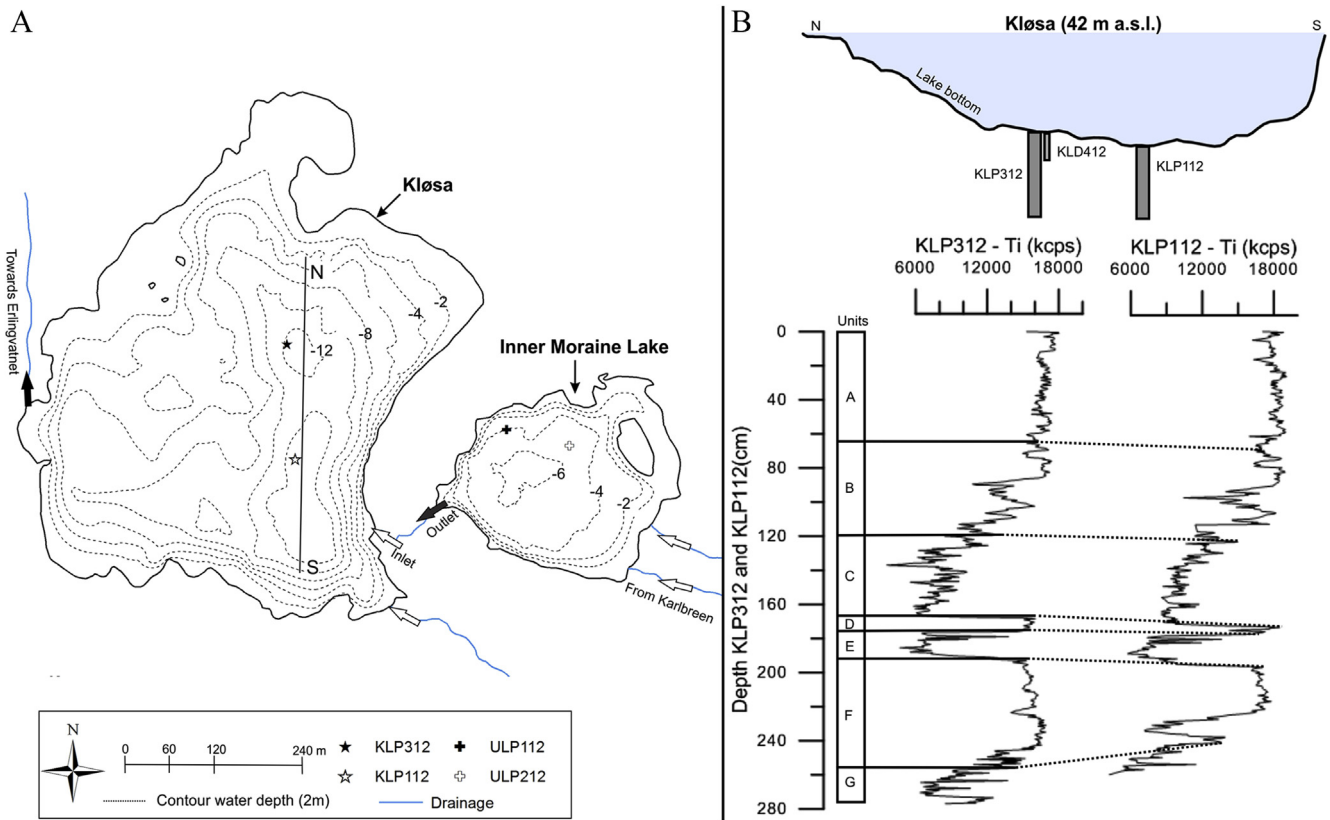
**Fig. 2.** A: Bathymetry of Kløsa and "Inner Moraine Lake" shown with coring locations. B: Transect showing the lake bathymetry along the vertical line in A, and coring locations. Sedimentary units have been correlated between the cores KLP312 and KLP112 using Ti kcps, as shown to the lower right.

indicates the transition from unit F to the overlying unit (E), where Ti count rates drops from ~16 200 to ~8000 kcps. The sharp lower boundary suggests that there is an erosional hiatus at the base of unit F and, together with the fining upwards sequence visually

observed in the sediments, indicates that the unit was deposited in one rapid event.

Laminated sediments dominate the entire E-unit (12 cm), ranging in size from thin (sub-mm) to thick (>mm) laminations. A
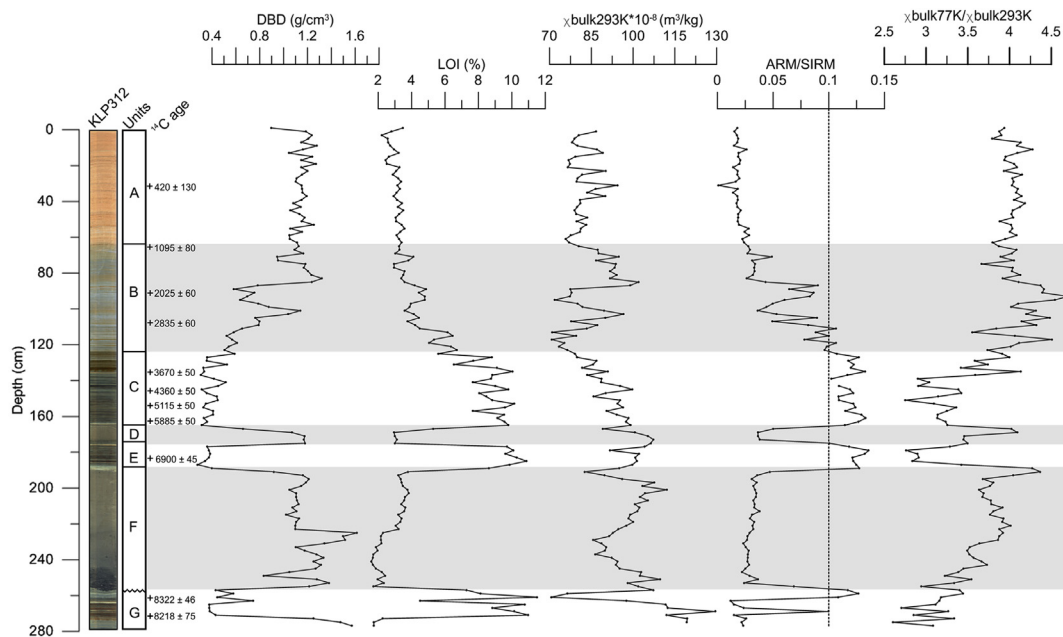


**Fig. 3.** Selected physical and magnetic parameters from KLP312. From left to right: core image of KLP312 with depth scale; the units found in KLP312 based on lithostratigraphy; position of radiocarbon dates; Dry bulk density (DBD); Loss-on-ignition (LOI); χbulk293 susceptibility; ARM/SIRM; χbulk77 K/χbulk293 K. All parameters are shown on two cm resolution. The presence of magnetotactic bacteria (MTB) in Kløsa is indicated by an ARM/SIRM ratio above 0.1, i.e. dotted vertical line (see text).
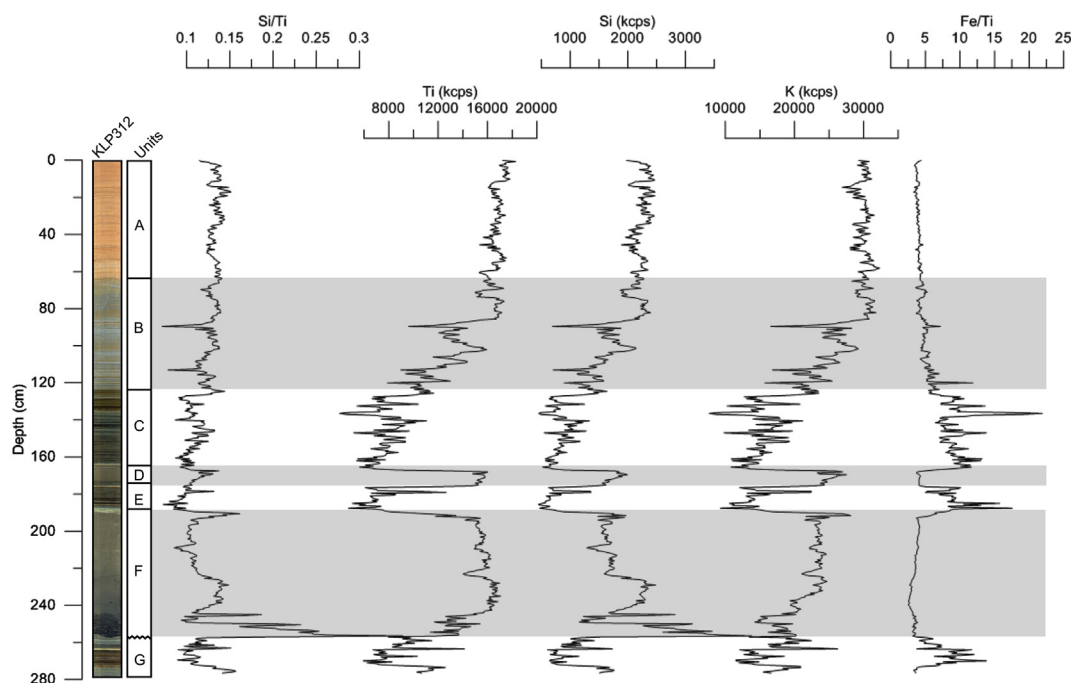
**Fig. 4.** Selected results from the ITRAX XRF surface scan resampled at 0.5 cm resolution (original resolution 200 μm). The results are shown in kilocounts-per-second (kcps).

distinct light-coloured layer (2 mm) stands out in between the dark olive grey and brown colours at 179 cm, which corresponds to a sharp increase in the geochemical elements Ti (from ~7000 to ~12 650 kcps), Si (from ~700 to ~1350 kcps) and K (from ~14 200 to ~22 400 kcps). Here, we find the highest LOI values (~10.8%) of the entire KLP312 core, which coincides with the lowest observed DBD (0.3 g/cm$^3$) values. The magnetic properties show a high average χBulk293 K values (~90*10$^{-8}$ m$^3$/kg) in the unit while the ARM/SIRM ratio stays above 0.1. Further, the Ti (~4750 kcps), Si (~450 kcps) and K (~9400 kcps) all show the lowest count rates found throughout KLP312 in this unit.

Unit D (10 cm) is characterised as a massive unit with a light grey brown colour, and a light band is found close to the top of the unit. Silt dominates the unit with a sand layer found at the top. The lithostratigraphy, physical-, magnetic-, and geochemical properties all show abrupt changes from the over- and underlying units, as illustrated by the sharp increase in count rates of Ti (from ~6000 to ~15 000 kcps), Si (from 624 to 1600 kcps) and K (from ~12 000 to ~24 300 kcps) at the bottom part of unit D (176 cm).

Alternating bands of black and lighter colours occur throughout unit C (41 cm), with the colour changing from an olive-grey background in the bottom of the unit to dark-brown at the top of the unit. The unit shows low average DBD values (~0.5 g/cm$^3$) with an opposite trend in the LOI values (8—10%) for the lower ~40 cm of this unit. The χBulk293 K values shows decreasing trend from the lower part towards the top of the unit, as the values drop from 100*10$^{-8}$ m$^3$/kg to ~80*10$^{-8}$ m$^3$/kg in the upper part. The average count rates of Ti (~8300), Si (~950), and K (~16 500) are low in the lowermost part of unit C compared to the rest of KLP312, with an abrupt spike in Ti and Si count rates at 136—136.5 cm. The Fe/Ti ratio shows high variations (from 5.5 to 22) with abrupt spikes throughout the unit.

Diffuse lamination of light brown colour is found in unit B (59 cm), with light grey colour dominating the entire unit. Unit B is characterised by a gradually increasing DBD, from 0.5 g/cm$^3$ to 1.3 g/cm$^3$, while an opposite pattern is seen in the LOI values, decreasing from ~10% to 4.5%. A similar pattern can be seen in the

Ti, K, and Si, with Ti count rates increasing from ~8000 kcps at the base of the unit to ~17 000 kcps at the top of the unit. A small decrease in the geochemical counts is seen between 101 cm and 89 cm with a distinct drop in Ti and Si values at 89.5—90 cm. Following this is a sharp increase towards the top of unit B. The ARM/SIRM ratio follows the same trend as it drops below 0.1 at 112 cm, and continues to decrease towards the top of the unit.

A distinct change in colour from light grey to light brown occurs at 65 cm, which marks the transition from unit B to A. Unit A (67 cm) is characterised by the highest DBD values (~1.2 g/cm$^3$) and count rates of Ti (~18 200 kcps), Si (~2500 kcps) and K (~32 300 kcps), and the lowest percentage of LOI and WC found throughout KLP312. The unit has little or no variation in the Fe/Ti ratio.

### 4.2. Age—depth model

The sparse amount of vegetation cover in the High-Arctic made it difficult to get sufficient amount of material for radiocarbon dating. However, as the two cores from Kløsa could easily be matched (Fig. 2) we were able to combine material from both cores in order to increase the sample sizes (Table 2). In general, the low amount of organic matter in the samples contributes to a larger uncertainty in samples with small amounts of organic carbon (e.g. sample LuS 10 776 in Table 2).

The result from the ^{14}C-dating revealed the sample ETH49511, marked by red star in Fig. 5, to be older than the sample found below. The sample was therefore excluded from the age—depth model due to its inverted age. The excluded sample is believed to be redeposited by in-wash from the catchment.

### 4.2.1. Episodic events

The data from KLP312 show how the units F and D differ significantly from the over- and underlying units, in terms of lithostratigraphic, physical and geochemical properties. Also, the borders between the over- and underlying units are sharp and abrupt. The undulating border between unit F and G indicates an erosive

**Table 2**
Radiocarbon dates from KLP312 and KLP112.

| Core | Lab. no | Depth (cm) | Material | mg C | Radiocarbon | Calibration age (cal. yr. BP) | |
|------|---------|-----------|----------|------|-------------|------|------|
| | | | | | ±1σ | 1σ | 2σ |
| KLP312 + 112 | LuS 10776 | 32.5 | Macrofossil | 0.08 | 420 ± 130 | 315–544 | 265–665 |
| KLP312 + 112 | LuS 10777 | 66.5 | Macrofossil | 0.09 | 1095 ± 80 | 928–1171 | 801–1234 |
| KLP312 + 112 | LuS 10778 | 93.5 | Macrofossil | 0.16 | 2025 ± 60 | 1899–2049 | 1868–2142 |
| KLP312 + 112 | LuS 10779 | 114.5 | Macrofossil | 0.18 | 2835 ± 60 | 2862–3030 | 2791–3140 |
| KLP312 + 112 | LuS 10780 | 135.0 | Macrofossil | 0.5 | 3670 ± 50 | 3927–4083 | 3871–4147 |
| KLP312 + 112 | LuS 10781 | 146.5 | Macrofossil | 0.74 | 4360 ± 50 | 4859–5025 | 4837–5212 |
| KLP312 + 112 | LuS 10782 | 156.5 | Macrofossil | 0.61 | 5115 ± 50 | 5755–5921 | 5740–5984 |
| KLP312 | LuS 10783 | 166.5 | Macrofossil | 0.73 | 5885 ± 50 | 6657–6775 | 6565–6845 |
| KLP312 | ETH49512 | 185.5 | Macrofossil | 0.21 | 6900 ± 45 | 7681–7784 | 7659–7839 |
| KLP312 | ETH49511 | 261.5 | Macrofossil | 0.21 | 8322 ± 46 | 9292–9421 | 9143–9466 |
| KLP312 | ETH49510 | 271.5 | Macrofossil | 0.08 | 8218 ± 75 | 9034–9286 | 9014–9404 |

contact and in turn a hiatus in the sediment record. Radiocarbon dates above and below the unit indicate unit F to have been deposited between 7737 (+105/−80) and 9197 (+210/−185) cal. yr. BP and unit D between 6707 (+140/−145) and 7737 (+105/−80) cal. yr. BP.

The relatively low LOI values and lack of macrofossils in the two units could indicate that they are the result of sub-aqueous processes, although the lack of macrofossils could also be explained by the generally low vegetation cover on Svalbard (Snyder et al., 1994). The normal grading found in the bottom part of unit F suggests that it was formed by a subaqueous high-density current, and the finer material towards the top might indicate that the depositional process evolved from a high-to low-density turbidity current (Lowe, 1982). Unit D is a massive unit with a sand layer at the top, which could reflect deposition by a non-turbulent debris flow.

Units D and F were removed from the data set prior to additional analyses, as we believe they represent periods of instantaneous deposition and are therefore not relevant to the study of the continuous sedimentation related to glacial input. Furthermore, it is necessary to remove them in order to obtain a correct age–depth model (Rubensdotter and Rosqvist, 2009). In addition to removing the two major units, we also removed four smaller layers (at 89.5–90 cm, 113–113.5 cm, 136–137 cm and 179–179.5 cm) which were interpreted as event layers based on abrupt spikes in the sediment parameters and their physical characteristics.

### 4.3. Principal component analysis

The result of the PCA reveals a strong, predominant signal in the sedimentary parameters of KLP312, as the first principal component axis (PCA1) explains 92% of the total variance in the data set. PCA2 has a much weaker explanatory power, capturing only 3% of the total variance, and is therefore not significant (Fig. I in Supplementary). A strong inverse correlation is seen between LOI and DBD, whereas the geochemical elements K, Al, Ti, Si and Rb show a high positive correlation with each other, as well as with DBD (Fig. 6 and Fig. I in Supplementary). The correlation with DBD indicates that the geochemical elements K, Al, Ti, Si, and Rb all reflect input of inorganic detrital material to the lake, and their high parameter scores along PCA1 suggest that this process is the main driver of the sedimentary signal in KLP312. The bulk magnetic susceptibility ($\chi$Bulk293 K) shows an inverse correlation with the indicators of inorganic detrital input. This implies that the magnetic signal is not carried by minerogenic particles transported into the lake from the catchment, but rather that it may be related to processes within the lake itself.

Because the physical proxies were sampled at a much lower resolution than the geochemical proxies, we used the PCA to identify which of the high-resolution geochemical elements best reflect the main sedimentary signal in the multi-proxy data set (i.e.
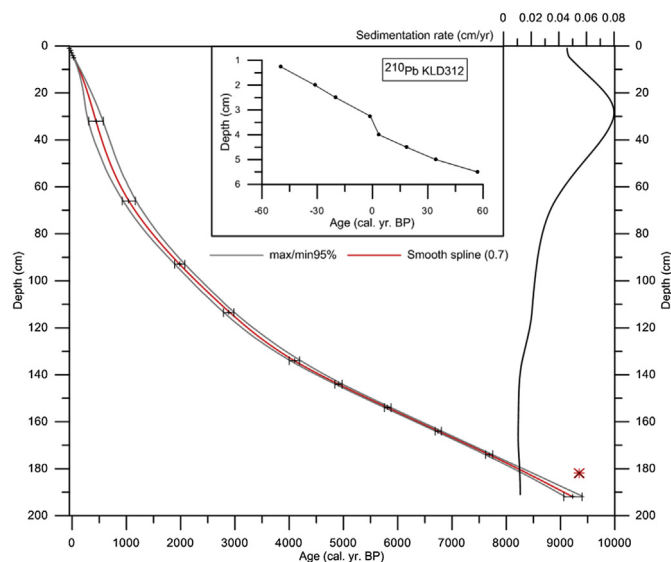


**Fig. 5.** The age–depth model is constructed using a smooth spline interpolation between the ^{210}Pb-dated sediments in the top of the core (upper 6 cm) and the radiocarbon dates from Table 2. The error bars indicate the 2σ uncertainty range for each radiocarbon sample. Units and event layers representing instantaneous sedimentation were removed prior to constructing the age–depth model (see Section 4.2), hence the new depth scale (y-axis). The reconstructed sedimentation rate (cm/yr) is shown on the right-hand side. Inlet plot shows the result from the ^{210}Pb dating of the uppermost sediments in KLD312, which can be directly matched with KLP312 (Fig. II in Supplementary material).
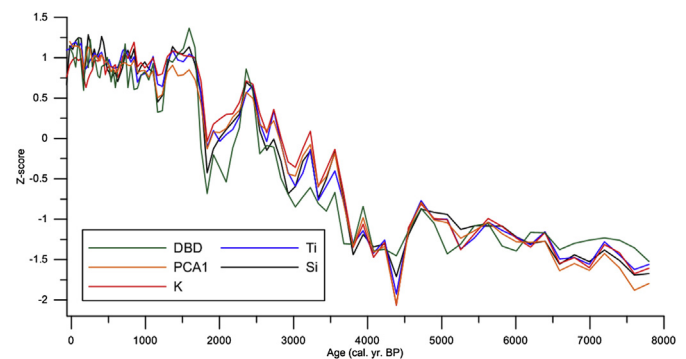


**Fig. 6.** Standardized values of DBD (dry-bulk-density), K (potassium), Ti (titanium) and Si (silicon) from KLP312 compared to variations along the first principal component axis (PCA1) of the entire data set (Fig. I in Supplementary material).

PCA1). Si is the element with highest score along the first principal component axis, and is therefore considered to be the single element that is most suitable as an indicator of inorganic sedimentary influx.

### 4.4. Erosion rates

For the purpose of calculating erosion rates, we assume that the sedimentary units identified in core KLP312 are draped uniformly over the area where we observe the laminated sedimentary infill in the GPR data (e.g. the sediment pack in profile 4 in Fig. V Supplementary material). From the age model we know that the sediments in unit C of KLP312 were deposited during a period of ~3300 years, and assuming a density of 2.65 g/cm$^3$ we obtain a mean porosity of 0.85. Using the equation from Section 3.6 this gives an average erosion rate of 0.0012 mm/yr across the entire catchment of Kløsa (including what is today sub-glacial). The upper 120 cm of KLP312 were deposited during the last ~3400 years, and has a mean porosity of 0.6, which gives an erosion rate of 0.0075 mm/yr during this time span.

The above indicates a sixfold increase in erosion rate during the last 3400 years relative to the preceding time period, and this increase is, as discussed further below, probably the result of Karlbreen reforming at the start of the Neoglacial. By using a mean glaciated area of 1 km$^2$, and by assuming that the erosion rate in the unglaciated part of the catchment remains unchanged, the estimated mean erosion rate below Karlbreen is approximately 0.02 mm/yr for the last 3400 years.

## 5. Discussion

Lakes are natural sinks for sediment delivered by various catchment processes, and in order to identify a 'glacier signal' in a distal glacier-fed lake it is necessary to evaluate all possible non-glacial processes that might produce deposits with a similar signature as glacier-derived sediments in the lake stratigraphy (Jansson et al., 2005; Rubensdotter and Rosqvist, 2009). For example, paraglacial re-adjustment of the landscape following a glacier's retreat could lead to mass-movement events, and erosion and re-deposition of glacier-derived sediments (Church and Ryder, 1972; Ballantyne, 2002).

### 5.1. Interpretation of the lacustrine sediment record

The geochemical elements Ti, Si, and K, together with DBD, are interpreted to reflect changes in the amount of inorganic detrital input to Kløsa (Fig. 6), and should therefore be sensitive to changes in the amount of glacial erosion in the upstream catchment. This is based on the general assumption that a larger glacier produces more minerogenic sediments compared to a smaller glacier (Leonard, 1997; Jansson et al., 2005; Bakke et al., 2010).

Above we concluded that Si is the most robust, high-resolution indicator of inorganic detrital input to Kløsa. Biogenic silica produced by diatoms (not observed in the sediments) could, however, be another possible source of Si (Kylander et al., 2011), and the possibility that the Si record in Kløsa is affected by changing biological productivity within the lake must therefore be considered. DBD, Ti, K, and variations along PCA1 all show a very similar trend to that of Si throughout KLP312 (Fig. 6), whereas LOI shows an opposite trend, which would not be expected if Si-content was driven by biological productivity. Furthermore, the potential influence of biogenic silica on the total Si count rate can be examined by normalising Si against an independent detrital indicator such as Ti (Croudace et al., 2006; Balascio et al., 2011). The Si/Ti-ratio shows little variation throughout most of KLP312 (Fig. 4), staying close to

0.1, and the similar behaviour of Si and Ti is also shown clearly in the PCA, where their parameter scores are virtually identical along both PCA1 and PCA2 (Fig. I in Supplementary material). Based on this, we rule out biogenic silica as a significant driver for the observed changes in Si-content.

The units E and C are characterised by the highest average LOI and WC values throughout KLP312, and the lowest average values seen for all of the abovementioned indicators of inorganic detrital input. Furthermore, the ratio between the redox-sensitive element Fe and the redox-insensitive element Ti is higher in these two units than in the rest of the core. This could either be associated with redox-related processes within the lake or to supply of sediments that have been exposed to sub-aerial conditions in the catchment of the lake. The former is associated with bottom water anoxia due to stratification of Kløsa during periods of low input of water to the lake and/or lowering of the lake level. The latter would favour a higher relative contribution from non-glacial sediment compared to detrital sediments to Kløsa.

### 5.2. Environmental magnetism

The ratio of χBulk measured at 77 K versus χBulk measured at 293 K (77 K/293 K) indicates that the magnetic susceptibility in units A and B are totally dominated by paramagnetic minerals, with a 77 K/293 K ratio close to 3.8 (Fig. 3). This could be explained by a high presence of biotite, a strongly paramagnetic mineral, in the local mica-schist bedrock. The lower 77 K/293 K ratio in units C and E imply that the samples contain some amount of ferri- or ferro-magnetic minerals, most likely magnetite. As was hinted at by the results of the PCA (Section 4.3), this pattern is not easily explained by changes in inorganic detrital input from the catchment, as the entire area is dominated by mica schist, but points toward processes occurring within the lake.

A possible explanation for the lowered 77 K/293 K ratio in units C and E could therefore be the presence of magnetite produced by magnetotactic bacteria (Fig. 3) (Stolz et al., 1990). This could explain why χBulk values correlate somewhat with LOI, as a general increase in the primary productivity of the lake would favour the formation of organic material in general, but also production of bacterial magnetite. A ratio greater than 0.1 between ARM and SIRM indicates biologically produced magnetite (Fig. 3), and hence indicate the presence of magnetotactic bacteria (MTB) in the lake (Paasche et al., 2004; Paasche and Løvlie, 2011). Supporting this is the positive relationship between ARM/SIRM and the S-ratio (IRM$_{0.1T}$/IRM$_{1T}$) from Kløsa (Fig. VII in Supplementary material). The S-ratio is an indicator of magnetic mineralogy and in units C and E the S-ratio stays close to 1, suggesting that magnetite dominates the magnetic mineralogy. Thus, when the conditions for magnetotactic bacteria in Kløsa change the S-ratio drops accordingly and indicates a change in the magnetic mineralogy of the sediments in units B and A.

Magnetotactic bacteria were therefore probably present in Kløsa from ~8400 to ~3000 cal. yr. BP. Because the optimal conditions for magnetotactic bacteria are close to the Oxic–Anoxic Transition Zone (Paasche and Larsen, 2010) this agrees well with the above-mentioned inference that anoxic conditions might have prevailed during this period, when runoff to the lake is low causing bottom water stratification. The termination of the MTB after ~3000 cal. yr. BP suggests a different lake regime dominating, and we suggest that increased summer runoff to Kløsa, in the form of melt water from Karlbreen, would cause a greater mixing of the water column, hence reducing the optimal conditions for MTB. The low sampling frequency (every 2 cm) makes it difficult to assess the accurate timing for the colonisation of Kløsa by magnetotactic bacteria. However, the proposed age of ~8400 cal. yr. BP is younger

than what was found for the synchronised colonisation by magnetotactic bacteria in four Norwegian lakes (9760 ± 160 cal. yr. BP) (Paasche and Løvlie, 2011).

### 5.3. Erosion rate of a subpolar glacier in the Arctic

The estimated mean erosion rate of 0.02 mm/yr by Karlbreen is low compared to the present erosion rates in Norway, Switzerland and Alaska reported by Hallet et al. (1996). Their compilation of data was based on observed erosion rates from the different sites and showed that the Norwegian glaciers varied between 0.038 and 0.48 mm/yr. A study from western Norway, Bødalsbreen, indicated a total erosion rate of 0.8 ± 0.4 mm/yr for the period AD 1650–1930 (Burki et al., 2010). This estimate is significantly higher than this study, and also greater than denudation rates obtained from sediments in Linnèvatnet, 0.015 mm/yr, during the Holocene (Svendsen et al., 1989).

Sub-glacial erosion rates are influenced by glacier size, dynamics and basal temperature, together with local conditions such as bedrock lithology and geomorphology. Over longer timescales these properties and conditions might change, which highlights the complexity of calculating glacier erosion rates (Burki et al., 2010). However, we might conclude that the appearance of Karlbreen in the catchment of Kløsa caused a significant shift in the lake's sedimentary regime, and that over the last 3400 years glacier erosion has most probably been the main source of detrital input to Kløsa.

### 5.4. Continuous ELA reconstruction

Because Karlbreen presently covers a significant portion of Kløsa's upstream catchment (area ratio 1:3.5), and from the estimated sub-glacial erosion rates, changes in the size of this cirque glacier will have a profound influence on the sedimentary budget of the lake. Above, we concluded that inorganic detrital input is the main driver of the sedimentary signal recorded in Kløsa (i.e. PCA1). Based on this, we infer that the sedimentary parameters reflecting input of inorganic detrital material will to a large extent also reflect changes in the size, and thus ELA, of the upstream glacier, and among the high-resolution geochemical parameters, Si count rates were found to best reflect the total sedimentary signal. Thus, by using historical ELA values for Karlbreen (see Table 3 and Fig. VI in Supplementary material) and the Si count rates at corresponding age levels in the dated sediment core, it is possible to construct a regression model (Fig. 7) describing the relationship between this sedimentary parameter and the ELA of Karlbreen. However, this relationship will only be valid as long as the glacier has actually existed, and it is likely that Karlbreen has been completely melted away in the past. Further, we also assume that the relationship between the ELA and sedimentary parameters in the recent past remain linear over longer timescales. The reconstructed ELA curve (Fig. 7) must be regarded only as a local ELA-reconstruction for Karlbreen, as wind and avalanches might rearrange the snow pack

**Table 3**
Calculated ELA's of Karlbreen using the AAR and the AABR methods, during the years 2008, 1990, 1966 and 1900.

| Year | AAR | AABR | ELA depression compared to present (m) |
|------|-----|------|----------------------------------------|
|      | 0.6 (±0.05) | 2.2 | |
| 2008 | 250 (±10) | 255 | – |
| 1990 | 240 (±10) | 240 | 15 |
| 1966 | 225 (±10) | 225 | 30 |
| 1900 | 200 (±20) | 190 | 65 |

and cause a leeward effect in the cirque. In turn, this impacts the mass balance of the glacier (Bakke and Nesje, 2011).

Other studies on Svalbard have demonstrated a warmer than present climate during the early Holocene (Birks, 1991; Salvigsen et al., 1992), and during this period glaciers on the western coast of Svalbard are believed to have been either absent or very small (Svendsen and Mangerud, 1997). In the record from Kløsa, the time period from 9200 to 4000 cal. yr. BP is characterised by minimum values in all sedimentary parameters reflecting inorganic detrital input (Fig. 6) and a low sedimentation rate (Fig. 5), which may suggest that Karlbreen was small or even absent. During this period the ELA is therefore assumed to have been above the top of the present-day glacier at ~500 m a.s.l. This has been added as an extra data-point in the regression model, using a minimum ELA value of 500 m a.s.l. and average Si count rates from the period 6700–4000 cal. yr. BP. The range between the two regression models, the minimum sensitivity (excluding the 500 m a.s.l. data-point) and the maximum sensitivity (including the 500 m a.s.l. data-point), will thereby define the uncertainty of the reconstructed ELA (grey area in Fig. 7).

The sediments in KLP312 reflect continuous deposition throughout units A to C, however, above we inferred that unit D and F was deposited during an episodic event. The final ELA reconstruction (Fig. 7) is therefore based only on the continuously deposited sediments extending from 6700 cal. yr. BP to the present.

### 5.5. Holocene glacier and climate history at Svalbard

#### 5.5.1. Deglaciation – 7750 cal. yr. BP
The results from Kløsa suggest that Karlbreen was melted away or considerable smaller than present due to the high LOI values and lower DBD values and Ti, Si, Ca count rates found in unit G compared to the rest of KLP312. The lowest radiocarbon-dated sample (271.5 cm depth) yields a result of ~9200 cal. yr. BP., which implies that the deglaciation of the area occurred prior to this.

It is suggested by Landvik et al. (2014) that the final deglaciation of Mitrahalvøya was constrained by the local valley topography. Prior to this the ice flowed across the Lillehookfjord towards the Krossfjorden Basin. Following retreat of the topographically dependent glaciers, local cirque glaciers remained on Mitrahalvøya and during this stage the bottom part of unit G may indicate that Karlbreen was present.

#### 5.5.2. 7750–4000 cal. yr. BP
The period from 7750 to 4000 cal. yr. BP is represented by low inorganic detrital input to Kløsa, indicated by several sedimentary parameters in KLP312 (Fig. 6). This suggests that Karlbreen might have been melted away during this time period. The sediment analyses revealed several event layers within this period, and also include the rapidly deposited unit D.

A lacustrine sediment record from Linnévatnet (~150 km to the south) indicate that Linnébreen was melted away during this period (Svendsen and Mangerud, 1997), and that July temperatures were ~1.5 °C higher than present on the west coast of Svalbard (Birks, 1991). Furthermore, warmer-than-present Atlantic sea water reached the north coast of Svalbard from 9400 to 5300 cal. yr. BP, as inferred by the presence of blue mussels (M. edulis), and indicates the climatic optimum on Svalbard (Salvigsen, 2002).

#### 5.5.3. 4000–2000 cal. yr. BP
A depression in the reconstructed ELA can be seen from ~3800 to ~2400 cal. yr. BP, where it is inferred to have lowered from about ~510 m a.s.l. to ~250 m a.s.l. over a period of ~1400 years. However, minor fluctuations do occur as the ELA rises at 3300 and
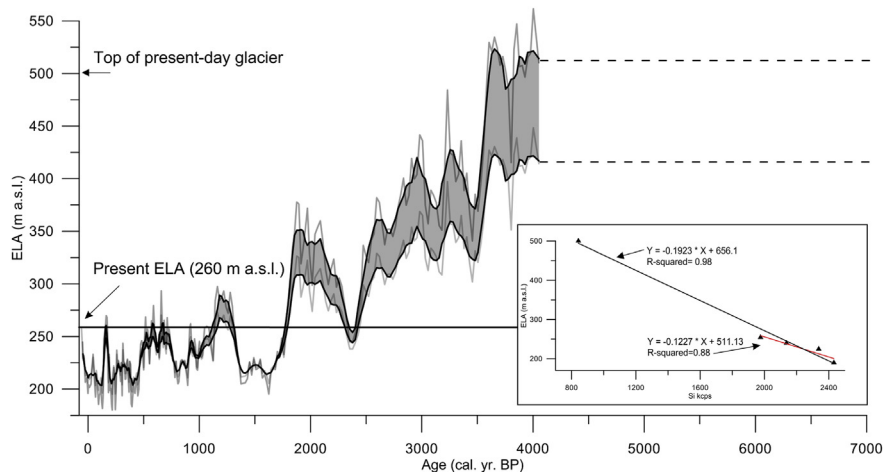
**Fig. 7.** Reconstructed equilibrium-line-altitude (ELA) for Karlbreen. The continuous ELA reconstruction is based on the Si record from Kløsa, which is transformed to ELA values through linear regression against past ELA estimates (inset figure). The ELA estimates are based on historical data (see Table 3) and the assumption that the ELA had to be lower than the top of the present-day glacier (500 m a.s.l.) when Karlbreen reformed at the start of the Neoglacial (~3800 cal. yr BP). For each point in time when the ELA is known, the altitude of the ELA can be plotted against the Si kcps value found at the corresponding time in the Kløsa sediment record (triangles, inset figure) and a regression can be made between them. Because the ELA estimate for the start of the Neoglacial is more uncertain than the historical data, two regression models were constructed: one using only historical data (red line, inset figure) and one using the 500 m a.s.l. ELA inferred for the start of the Neoglacial in addition to the historical data (black line, inset figure). Reconstructions based on both models are shown in the ELA plot (black line = 5 year running mean), and the difference between them is shown with grey shading. The lower horizontal line represents the present ELA of Karlbreen using the AABR method (BR = 2.2). The two dotted lines represent the period where Karlbreen is interpreted to have been very small or completely melted away.

3000 cal. yr. BP. The distinct depression in Karlbreen's ELA between 3800 and 3500 cal. yr. BP corresponds with the regrowth of Linnébreen, after the HTM (Svendsen and Mangerud, 1997). Furthermore, the regrowth of Karlbreen and Linnébreen are in phase with the onset of the Neoglacial period in the Northern Hemisphere from around 4000 cal. yr. BP (Bakke et al., 2010). The Skardtjørna pollen record from the west coast of Svalbard, close to Linnèbreen, indicates a climatic cooling between 4000 and 2500 cal. yr. BP (Birks, 1991) and also supports our ELA reconstruction.

### 5.5.4. 2000 cal. yr. BP to present day

A distinct drop in the ELA occurred at ~1900 cal. yr. BP, when the ELA of Karlbreen dropped from ~340 to ~205 m a.s.l. This rapid depression in the ELA indicates that Karlbreen may have reached or been close to its maximum Holocene extent already around 1700 cal. yr. BP. Following this, Karlbreen retreated, as the reconstructed ELA rises abruptly between 1400 and 1200 cal. yr. BP. During this period, Karlbreen was probably behind its present limits. A study of [10]Be surface exposure ages on moraine boulders in the forefield of Linnébreen shows that the glacier was close to its maximum extent sometime between 4600 and 1600 cal. yr. BP and started to retreat after 1600 cal. yr. BP (Reusche et al., 2014). The timing between the two sites falls within the dating uncertainties of the methods applied, and it remains possible that the advance of Karlbreen around 1900 cal. yr. BP occurred as a response to a regional climatic shift along the western coast of Svalbard.

At ~1150 cal. yr. BP the reconstructed ELA gradually lowers from ~280 to 220 m a.s.l. In the corresponding period Humlum et al. (2005) recognised an advance of the glacier Longyearbreen, situated close to Longyearbyen. Here, preserved mosses were found ~2 km upstream from the present glacier front and dated to 1100 cal. yr. BP, indicating a significant glacier advance around this time. Werner (1993) suggests moraine stabilisation occurred on the west coast of Svalbard, between 550 and 700 cal. yr. BP, which corresponds to the rise in Karlbreen's ELA following the advance between 1150 and 850 cal. yr. BP.

The Neoglacial period on Svalbard culminated during the LIA, when the largest Holocene glacier extent is in general thought to

have occurred on Svalbard (Werner, 1993; Svendsen and Mangerud, 1997; Snyder et al., 2000). The ELA of Karlbreen was close to its lowest extent at ~400, ~230 and ~130 cal. yr. BP, with the ELA staying close to 200 m a.s.l. towards the beginning of the 20th century. This suggests that the LIA period on Svalbard lasted from 450 cal. yr. BP to the start of the 20th century.

A distinct rise in the ELA from ~205 to 260 m a.s.l. occurred between 225 and 135 cal. yr. BP, separating the LIA period into two intervals. A two-step model of glacier advances on Svalbard has previously been suggested by Werner (1993), and Svendsen and Mangerud (1997) who argued for a period of distinct warming from 200 to 250 cal. yr. BP. This was addressed by Gordiyenko et al. (1981) in their study of ice-cores from the Lomonosov Plateau. The palaeoclimatic reconstructions, derived from $\delta^{18}O$ values, showed a warming in the eighteenth century (Gordiyenko et al., 1981), which corresponds with the distinct rise in Karlbreen's ELA during this interval. A similar distinct warming was identified by D'Andrea et al. (2012) mid-18th century from their $U_{37}^K$ temperature reconstruction of Kongressvatnet.

The trend from 50 cal. yr. BP to the present day indicates a steady rise in Karlbreen's ELA, and implies a retreat of the glacier since the latest LIA maximum in the early twentieth century. The formation of "Inner Moraine Lake" by the ice-cored moraine (Fig. 1B), occurred after this final retreat of Karlbreen, and the sedimentation in the small lake reveals continuous deposition for at least thirty years (Fig. III in Supplementary material).

### 5.6. Ice-cored moraine

The reconstruction of the ELA of Karlbreen suggests that the glacier was close to or at its maximum extent several times during the last 1700 years (i.e., at or close to the ice-cored moraine shown in Fig. 1B). The undisturbed sediments and continuous sedimentation during the past 6700 years recorded in KLP312 have implications concerning the origin of the ice-cored moraine extending into Kløsa. Studies have previously shown that an ice-cored moraine could potentially survive for several millennia, due to the preservation effect of thick debris covers (Dyke and Savelle, 2000). In permafrost regions, the debris cover can exceed the

active-layer thickness, which in turn will result in a limited melt rate of the in-situ ice (Schomacker and Kjær, 2007).

The results from the GPR survey in Kløsa show how the laminated sediments are draped on top of the chaotic sediments close to the margin of Kløsa. The profile runs from the margin of Kløsa where the ice-cored moraine runs into the lake and towards the middle part of the lake (see Fig. V in Supplementary material). We argue that the continuous, undisturbed sedimentation in Kløsa requires a minimum age of 6700 years for the ice-cored moraine formation, because it is likely that any event (e.g., a slumping event) from the steep distal side of the moraine would have created a distinct signature in the sediment record. This implies that the ice-cored moraine initially formed before 6700 cal. yr. BP and has later been modified by several glacier advances where Karlbreen has been close to or at the moraine margin during the Neoglacial time period. The picture in Fig. IV (Supplementary material) from the northern side of the ice-cored moraine indicates a minimum of four stages, indicated by the red lines, representing periods when Karlbreen reached the ice-cored moraine.

If correct, it would suggest that the ice-cored moraine predates the Holocene Thermal Maximum (HTM), and the ice-cored moraine most likely was formed during the Younger Dryas or during a cold spell in the early Holocene. As the sediments in the basal parts of KLP312 and other regional climatic records suggest a warmer-than-
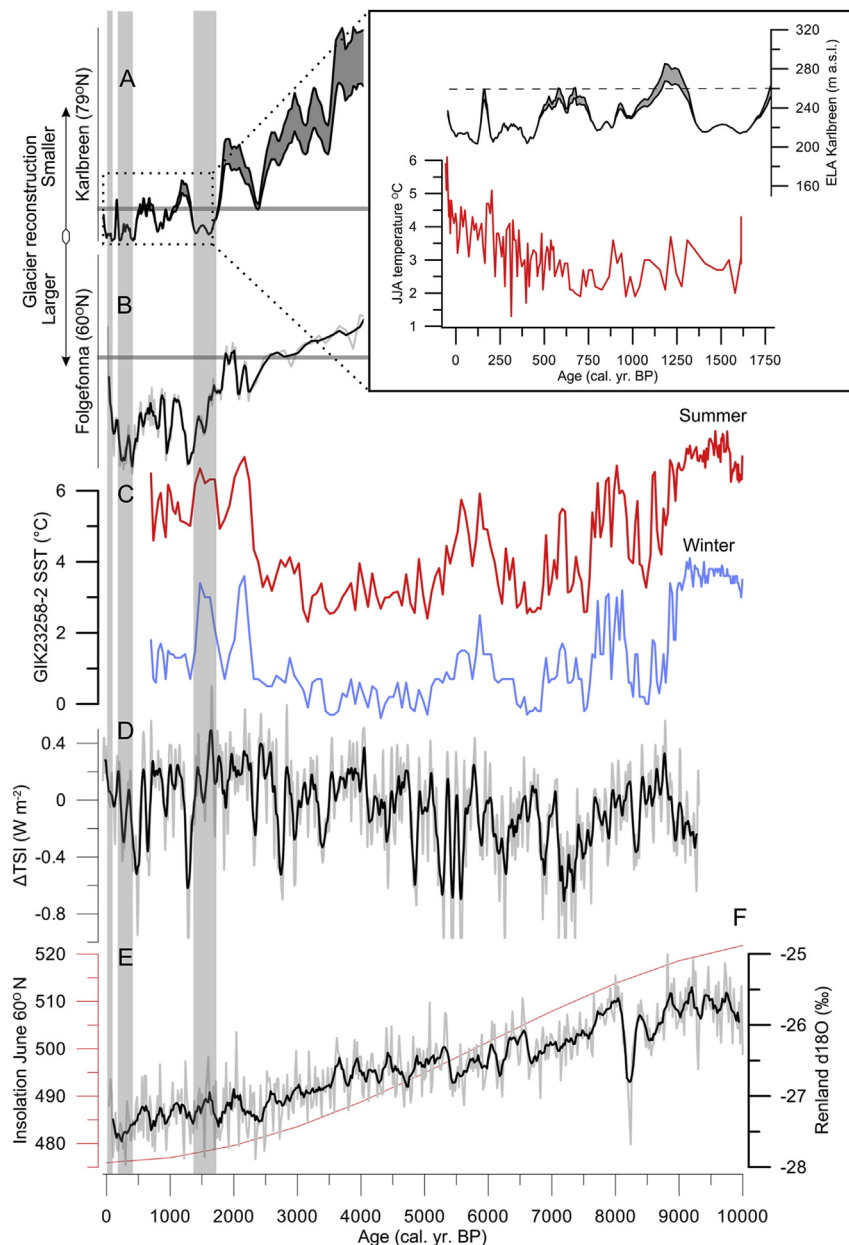


**Fig. 8.** Compilation of selected data sets and proxy records from the North Atlantic region: A) Reconstructed ELA curve (bold line: 5 pt. running mean) from Karlbreen (this study); B) Reconstructed ELA curve (bold line: 3 pt. running mean) from northern Folgefonna (Bakke et al., 2005); C) marine record from northern Norwegian Sea showing reconstructed sea-surface temperature during summer and winter (Sarnthein et al., 2003); D) The average Total solar irradiance (TSI) relative to the solar cycle minimum of the year AD 1986, shown using a 15 pt. running mean (bold line) (Steinhilber et al., 2009); E) June insolation at 60° N (Berger and Loutre, 1991); F) The δ18O data obtained from an ice-core on Renland, Greenland (Vinther et al., 2008). The grey vertical bands represent periods when Karlbreen was close to or at its maximum extent during the Neoglacial. Uppermost inset figure shows a comparison between the reconstructed ELA of Karlbreen (black line) and temperature reconstruction (red line) from Kongressvatnet (D'Andrea et al., 2012) during the last 1800 years.

present climate during the HTM, which consequently limits any potential glacier advance during this period (Birks, 1991; Svendsen and Mangerud, 1997; Salvigsen, 2002). In turn, the warmer-than-present conditions during the HTM on Svalbard could have caused melting of the ice within the moraine, resulting in the episodic events found in the sediment record from Kløsa (units D and F) dated to occur between 6700 and 9250 cal. yr. BP.

In contrast to this, local glaciers have previously been inferred to have been smaller in the YD than during the LIA-period on the west coast of Svalbard (Salvigsen, 1979; Mangerud and Svendsen, 1990; Mangerud and Landvik, 2007). A possible explanation for this could be moisture starvation on the west coast of Svalbard during the YD (Mangerud and Landvik, 2007). In such a scenario, climate was dry due to prevailing winds from the east over Svalbard, leaving the west coast in a lee-position and in a precipitation shadow from the polar easterlies (Birgel and Hass, 2004). The findings from Kløsa suggest that the formation of the ice-cored moraine has occurred in several stages, and the continuous sediments in KLP312 suggest a minimum age of the outermost moraine to be 6700 cal. yr. BP. This implies that Karlbreen was most likely close to, or at, its largest extent also sometime prior to the HTM on Svalbard. The use of other methods, like for example [10]Be dating on bedrock distal of the ice-cored moraine, could help to better constrain the age of the outermost moraine stage.

### 5.7. Climatic implications

The global cooling trend of the last 6000 years can be seen as a response to declining summer insolation (Fig. 8e) at high northern latitudes (Wanner et al., 2008). The mid-to-late Holocene behaviour of Karlbreen seems to have been a response to this declining summer insolation. This coincides with the overall trend in the North Atlantic (Fig. 8), with the development of glaciers in Scandinavia (Bakke et al., 2005, 2010), lower SSTs (reconstructed from work on the marine core MD95-2011 from Vøringplatået) (Berner et al., 2010), lower temperatures derived from $\delta^{18}O$ values in the Renland ice-core (Vinther et al., 2008) and lower summer temperatures reconstructed from terrestrial pollen records (Bjune and Birks, 2008). Superimposed on the general cooling trend is the variability in total solar irradiance ($\delta$TSI) (Steinhilber et al., 2009) which may, together with volcanism, have influenced the short-term variability of Karlbreen.

#### 5.7.1. The role of summer temperatures and winter precipitation on Svalbard glaciers

During the HTM, glaciers on Svalbard retreated, and many of them most likely vanished, as the summer temperatures were 1–2 °C higher than they are today (Birks, 1991; Salvigsen, 2002). Due to the near freezing level of summer temperatures on Svalbard, even small perturbations in the temperature may have large consequences for summer ablation rates on the glaciers (Lubinski et al., 1999). However, on a shorter timescale, D'Andrea et al. (2012) show how winter precipitation might have been an important factor in the latest glacier advance (within the last 250 years) on Svalbard. Their work on Kongressvatnet, close to Isfjord Radio, suggested 1–2.5 °C warmer summer air temperatures than during the previous glacier expansion on Svalbard, implying that higher ablation rates occurred during a period when the glaciers were expanding, requiring increased accumulation to provide a positive mass-balance (D'Andrea et al., 2012).

The impact of feedback mechanisms at higher latitudes (e.g. sea ice, albedo effect) complicates the picture of how winter precipitation and summer ablation influences Svalbard glaciers. Müller et al. (2012) propose that the northward retreat of the sea ice cover, triggered by a temporally strengthened West Spitsbergen

Current and/or change in the atmospheric circulation pattern, could cause abrupt glacier advances. Supporting this is the abrupt increase in SST at the continental margin of the Barents Sea at ~2200 and ~1700 cal. yr. BP (Sarnthein et al., 2003). This coincides with Karlbreen being at, or close to, its largest extent from ~1700 to ~1500 cal. yr. BP (Fig. 8c). The open waters on the west coast of Svalbard may have acted as a moisture source for Karlbreen during this period, implying that winter precipitation may be dominant in the annual mass-balance of the maritime glaciers along the western coast of Svalbard.

#### 5.7.2. Future perspectives

Today, the persistent retreat of glaciers on Svalbard since the LIA (documented by aerial photos and mass balance measurements) is most likely linked to higher summer temperatures and ablation rates exceeding the accumulation rate (Lefauconnier and Hagen, 1990; Hagen et al., 1993; Bruland and Hagen, 2002). Model simulations of glaciers close to Ny-Ålesund indicate that a cooling of 1.2–1.3 °C or a 100% increase in precipitation is required for the glaciers to remain in a steady state with the climate (Bruland and Hagen, 2002).

The current global warming is amplified in the Arctic, and also for the future scenarios, CMIP5 models indicate a mean warming of 2.2–2.4 times the mean global warming for the period 2081–2100, although the warming is constrained to the fall, winter and spring (Collins et al., 2013). The effect of longer seasonal open waters around Svalbard may well give increased moisture supply to the glaciers on the western coast, thereby moderating the effect of increased summer ablation rates, although some model simulations show that this effect may be very small (Day et al., 2012).

## 6. Summary and conclusions

The above findings are based on geomorphological mapping in addition to a GPR-survey and multi-proxy analyses of a robustly dated lacustrine sediment record from Kløsa.

The continuous sediment record extends back to 6700 cal. yr. BP. The onset of the local Neoglacial period occurred at ~3500 cal. yr. BP as the reconstructed ELA shows a distinct lowering. Karlbreen was close to or at its maximum position several times during the Neoglacial (at 1700, 230 and 130 cal. yr. BP). The present warming in the Arctic has led to a rise in the ELA of Karlbreen during the twentieth century.

The long-term trend in the extent of Karlbreen corresponds to the regional climatic pattern in and around the North Atlantic. Here, the declining summer insolation which led to cooling seems to be the driving factor for the last 6000 years. Sea-ice distribution is thought to have impacted the moisture supply, especially during the advance at ~1700 cal. yr. BP. Although summer ablation has probably played a significant role in the net balance of glaciers on Svalbard in the past 8000 years (Baranowski and Karlén, 1976; Werner, 1993), it is proposed here that the retreat of the sea-ice might have provided more moisture for the glaciers on the western coast of Svalbard during certain time periods.

A minimum age of 6700 years has been suggested for the ice-cored moraine, as no perturbations are registered in the sediment record from Kløsa following this time. Evidence from the GPR-survey, together with field observations of several stages of moraine development, has led us to conclude that the ice-cored moraine in front of Karlbreen is the result of several glacier advances during the late-Holocene. In turn, this implies that the outermost moraine stage formed before the HTM, and given the warmer-than present conditions during the HTM the ice-cored moraine is the likely source for the episodic events found in unit D and F.

## Appendix A. Supplementary data

Supplementary data related to this article can be found at http://dx.doi.org/10.1016/j.quascirev.2014.11.017.

## References

AMAP, 2011. Snow, Water, Ice and Permafrost in the Arctic (SWIPA). Arctic Monitoring and Assessment Programme (AMAP), Oslo.

Bakke, J., Dahl, S.O., Paasche, O., Simonsen, J.R., Kvisvik, B., Bakke, K., Nesje, A., 2010. A complete record of Holocene glacier variability at Austre Okstindbreen, northern Norway: an integrated approach. Quat. Sci. Rev. 29, 1246–1262.

Bakke, J., Lie, O., Heegaard, E., Dokken, T., Haug, G.H., Birks, H.H., Dulski, P., Nilsen, T., 2009. Rapid oceanic and atmospheric changes during the Younger Dryas cold period. Nat. Geosci. 2, 202–205.

Bakke, J., Lie, O., Nesje, A., Dahl, S.O., Paasche, O., 2005. Utilizing physical sediment variability in glacier-fed lakes for continuous glacier reconstructions during the Holocene, northern Folgefonna, western Norway. Holocene 15, 161–176.

Bakke, J., Nesje, A., 2011. Equilibrium-Line Altitude (ELA). In: Singh, V., Singh, P., Haritashya, U. (Eds.), Encyclopedia of Snow, Ice and Glaciers. Springer-Verlag Berling Heidelberg. Springer Reference. www.springerreference.com.

Bakke, J., Paasche, Ø., 2011. Sediment core and glacial environment reconstruction. In: Singh, P., Singh, V., Haritashya, U. (Eds.), Encyclopedia of Snow, Ice and Glaciers. Springer-Verlag Berling Heidelberg. Springer Reference. www.springerreference.com.

Bakke, J., Trachsel, M., Kvisvik, B.C., Nesje, A., Lyså, A., 2013. Numerical analyses of a multi-proxy data set from a distal glacier-fed lake, Sørsendalsvatn, western Norway. Quat. Sci. Rev. 73, 182–195.

Balascio, N.L., Zhang, Z., Bradley, R.S., Perren, B., Dahl, S.O., Bakke, J., 2011. A multi-proxy approach to assessing isolation basin stratigraphy from the Lofoten Islands, Norway. Quat. Res. 75, 288–300.

Ballantyne, C.K., 2002. Paraglacial geomorphology. Quat. Sci. Rev. 21, 1935–2017.

Ballantyne, C.K., Benn, D.I., 1994. Paraglacial slope adjustment and resedimentation following recent glacier retreat, Fåbergstølsdalen, Norway. Arct. Alp. Res. 26, 255–269.

Baranowski, S., Karlén, W., 1976. Remnants of Viking Age Tundra in Spitsbergen and Northern Scandinavia. Geogr. Ann. Ser. A Phys. Geogr. 58, 35–40.

Benn, D., Evans, D., 2010. Glaciers and Glaciation, second ed. Hodder Arnold Publication.

Benn, D.I., Lehmkuhl, F., 2000. Mass balance and equilibrium-line altitudes of glaciers in high-mountain environments. Quat. Int. 65, 15–29.

Berger, A., Loutre, M.-F., 1991. Insolation values for the climate of the last 10 million years. Quat. Sci. Rev. 10, 297–317.

Berner, K.S., Koç, N., Godtliebsen, F., 2010. High frequency climate variability of the Norwegian Atlantic Current during the early Holocene period and a possible connection to the Gleissberg cycle. Holocene 20, 245–255.

Birgel, D., Hass, H.C., 2004. Oceanic and atmospheric variations during the last deglaciation in the Fram Strait (Arctic Ocean): a coupled high-resolution organic-geochemical and sedimentological study. Quat. Sci. Rev. 23, 29–47.

Birks, H., 1987. Multivariate analysis of stratigraphic data in geology: a review. Chemom. Intell. Lab. Syst. 2, 109–126.

Birks, H.H., 1991. Holocene vegetational history and climatic change in west Spitsbergen – plant macrofossils from Skardtjørna, an Arctic lake. Holocene 1, 209–218.

Bjune, A.E., Birks, H.J.B., 2008. Holocene vegetation dynamics and inferred climate changes at Svanåvatnet, Mo i Rana, northern Norway. Boreas 37, 146–156.

Blaauw, M., 2010. Methods and code for 'classical' age-modelling of radiocarbon sequences. Quat. Geochronol. 5, 512–518.

Bruland, O., Hagen, J.O., 2002. Glacial mass balance of Austre Brøggerbreen (Spitsbergen), 1971–1999, modelled with a precipitation-run-off model. Polar Res. 21.

Burki, V., Hansen, L., Fredin, O., Andersen, T.A., Beylich, A.A., Jaboyedoff, M., Larsen, E., Tønnesen, J.F., 2010. Little Ice Age advance and retreat sediment budgets for an outlet glacier in western Norway. Boreas 39, 551–566.

Church, M., Ryder, J.M., 1972. Paraglacial sedimentation: a consideration of fluvial processes conditioned by glaciation. Geol. Soc. Am. Bull. 83, 3059–3072.

Collins, M., Knutti, R., Arblaster, J., Dufresne, J.-L., Fichefet, T., Friedlingstein, P., Xuejie, G., Gutowski, W.J., Johns, T., Krinner, G., Shongwe, M., Tebaldi, C., Weaver, A., Wehner, M., 2013. Long-term climate change: projections, commitments and irreversibility. In: Stocker, T., Qin, D., Plattner, G., Tignor, M., Allen, S., Boschung, J., Nauels, A., Xia, Y., Bex, V., Midgley, P. (Eds.), Climate Change 2013: the Physical Science Basis, Contribution of Working Group I to the Fifth Assessment Report of the Intergovernmental Panel on Climate Change. Cambridge University Press, Cambridge, United Kingdom and New York, NY, USA.

Croudace, I.W., Rindby, A., Rothwell, R.G., 2006. ITRAX: Description and Evaluation of a New Multi-function X-ray Core Scanner. In: Special Publication – Geological Society of London 267, p. 51.

D'Andrea, W.J., Vaillencourt, D.A., Balascio, N.L., Werner, A., Roof, S.R., Retelle, M., Bradley, R.S., 2012. Mild Little Ice Age and unprecedented recent warmth in an 1800 year lake sediment record from Svalbard. Geology 40, 1007–1010.

Dahl, S.O., Bakke, J., Lie, Ø., Nesje, A., 2003. Reconstruction of former glacier equilibrium-line altitudes based on proglacial sites: an evaluation of approaches and selection of sites. Quat. Sci. Rev. 22, 275–287.

Dahl, S.O., Nesje, A., 1992. Paleoclimatic implications based on equilibrium-line altitude depressions of reconstructed Younger Dryas and Holocene cirque glaciers in inner Nordfjord, western Norway. Palaeogeogr. Palaeoclimatol. Palaeoecol. 94, 87–97.

Davis, P.T., Menounos, B., Osborn, G., 2009. Holocene and latest Pleistocene alpine glacier fluctuations: a global perspective. Quat. Sci. Rev. 28, 2021–2033.

Day, J.J., Bamber, J.L., Valdes, P.J., Kohler, J., 2012. The impact of a seasonally ice free Arctic Ocean on the temperature, precipitation and surface mass balance of Svalbard. Cryosphere 6, 35–50.

Dean, W.E., 1974. Determination of carbonate and organic matter in calcareous sediments and sedimentary rocks by loss on ignition: comparison with other methods. J. Sediment. Petrol. 44, 242–258.

Divine, D., Isaksson, E., Martma, T., Meijer, H.A.J., Moore, J., Pohjola, V., van de Wal, R.S.W., Godtliebsen, F., 2011. Thousand years of winter surface air temperature variations in Svalbard and northern Norway reconstructed from ice core data. Polar Res. 30.

Dyke, A.S., Savelle, J.M., 2000. Major end moraines of Younger Dryas age on Wollaston Peninsula, Victoria Island, Canadian Arctic: implications for paleoclimate and for formation of hummocky moraine. Can. J. Earth Sci. 37, 601–619.

Forman, S.L., 1990. Post-glacial relative sea-level history of northwestern Spitsbergen, Svalbard. Geol. Soc. Am. Bull. 102, 1580–1590.

Førland, E., Hanssen-Bauer, I., 2000. Increased precipitation in the Norwegian Arctic: true or False? Clim. Change 46, 485–509.

Førland, E.J., Benestad, R., Hanssen-Bauer, I., Haugen, J.E., Skaugen, T.E., 2011. Temperature and precipitation development at svalbard 1900–2100. Adv. Meteorol. 2011, 14.

Førland, E.J., Benestad, R.E., Flatøy, F., Hanssen-Bauer, I., Haugen, J.E., Isaksen, K., Sorteberg, A., Ådlandsvik, B., 2010. Klimautvikling i Nord-Norge og på Svalbard i perioden 1900–2100: klimaendringer i norsk Arktis : NorACIA delutredning 1. Norsk polarinstitutt.

Glasser, N.F., Hambrey, M.J., 2005. Ice-marginal terrestrial landsystems: svalbard polythermal glaciers. In: Evans, D.J.A. (Ed.), Glacial Landsystem. Hodder Arnold, London.

Gordiyenko, F., Kotlyakov, V., Punning, Y.K., Vairmäe, R., 1981. Study of a 200-m core from the lomonosov ice plateau on spitsbergen and the paleoclimatic implications. Polar Geogr. 5, 242–251.

Hagen, J.O., Liestøl, O., 1990. Long-term glacier mass-balance investigations in Svalbard, 1950–88. Ann. Glaciol. 14.

Hagen, J.O., Liestøl, O., Roland, E., Jørgensen, T., 1993. Glacier Atlas of Svalbard and Jan Mayen. Norsk Polarinsitutt, Oslo.

Hagen, J.O., Melvold, K., Pinglot, F., Dowdeswell, J.A., 2003. On the net mass balance of the glaciers and ice caps in Svalbard, Norwegian Arctic. Arct. Antarct. Alp. Res. 35, 264–270.

Hallet, B., Hunter, L., Bogen, J., 1996. Rates of erosion and sediment evacuation by glaciers: a review of field data and their implications. Glob. Planet. Change 12, 213–235.

Heiri, O., Lotter, A.F., Lemchke, G., 2001. Loss on ignition as a method for estimating organic and carbonate content in sediments: reproducibility and comparability of results. J. Paleolimnol. 25, 101–110.

Hormes, A., Gjermundsen, E.F., Rasmussen, T.L., 2013. From mountain top to the deep sea – deglaciation in 4D of the northwestern Barents Sea ice sheet. Quat. Sci. Rev. 75, 78–99.

Humlum, O., Elberling, B., Hormes, A., Fjordheim, K., Hansen, O.H., Heinemeier, J., 2005. Late-Holocene glacier growth in Svalbard, documented by subglacial relict vegetation and living soil microbes. Holocene 15, 396–407.

Jansson, P., Rosqvist, G., Schneider, T., 2005. Glacier fluctuations, suspended sediment flux and glacio-lacustrine sedimensts. Geogr. Ann. Ser. A Phys. Geogr. 87, 37–50.

Jessen, S.P., Rasmussen, T.L., Nielsen, T., Solheim, A., 2010. A new Late Weichselian and Holocene marine chronology for the western Svalbard slope 30,000–0 cal years BP. Quat. Sci. Rev. 29, 1301–1312.

Karlèn, W., 1976. Lacustrine sediments and tree-line variations as indicators of climate flucutations in Lappland, northern Sweden. Geogr. Ann. 58, 273–281.

Kylander, M.E., Ampel, L., Wohlfarth, B., Veres, D., 2011. High-resolution X-ray fluorescence core scanning analysis of Les Echets (France) sedimentary sequence: new insights from chemical proxies. J. Quat. Sci. 26, 109–117.

König, M., Kohler, J., Nuth, C., 2013. Glacier Area Outlines – Svalbard. Norwegian Polar Institute, Tromsø.

Lanci, L., Lowrie, W., 1997. Magnetostratigraphic evidence that 'tiny wiggles' in the oceanic magnetic anomaly record represent geomagnetic paleointensity variations. Earth Planet. Sci. Lett. 148, 581–592.

Landvik, J.Y., Alexanderson, H., Henriksen, M., Ingólfsson, Ó., 2014. Landscape imprints of changing glacial regimes during ice-sheet build-up and decay: a conceptual model from Svalbard. Quat. Sci. Rev. 92, 258–268.

Lefauconnier, B., Hagen, J., 1990. Glaciers and climate in Svalbard: statistical analysis and reconstruction of the Brøggerbreen mass balance for the last 77 years. Ann. Glaciol. 14, 148–152.

Leonard, E., 1997. The relationship between glacial activity and sediment production: evidence from a 4450-year varve record of neoglacial sedimentation in Hector Lake, Alberta, Canada. J. Paleolimnol. 17, 319–330.

Lepš, J., Šmilauer, P., 2003. Multivariate Analysis of Ecological Data Using CANOCO. Cambridge University Press, New York.

Lie, Ø., Dahl, S.O., Nesje, A., Matthews, J.A., Sandvold, S., 2004. Holocene fluctuations of a polythermal glacier in high-alpine eastern Jotunheimen, central-southern Norway. Quat. Sci. Rev. 23, 1925–1945.

Lowe, D.R., 1982. Sediment gravity flows; II, Depositional models with special reference to the deposits of high-density turbidity currents. J. Sediment. Res. 52, 279–297.

Lubinski, D.J., Forman, S.L., Miller, G.H., 1999. Holocene glacier and climate fluctuations on Franz Josef Land, Arctic Russia, 80 N. Quat. Sci. Rev. 18, 85–108.

Lukas, S., 2011. Ice-cored moraines. In: Singh, V., Singh, P., Haritashya, U. (Eds.), Encyclopedia of Snow, Ice and Glaciers. Springer-Verlag Berling Heidelberg. Springer Reference. www.springerreference.com.

Mangerud, J., Landvik, J.Y., 2007. Younger Dryas cirque glaciers in western Spitsbergen: smaller than during the Little Ice Age. Boreas 36, 278–285.

Mangerud, J., Svendsen, J.I., 1990. Deglaciation chronology inferred from marine sediments in a proglacial lake basin, western Spitsbergen, Svalbard. Boreas 19, 249–272.

Masson-Delmotte, V., Schulz, M., Abe-Ouchi, A., Beer, J., Ganopolski, A., González Rouco, J.F., Jansen, E., Lambeck, K., Luterbacher, J., Naish, T., Osborn, T., Otto-Bliesner, B., Quinn, T., Ramesh, R., Rojas, M., Shao, X., Timmermann, A., 2013. Information from Paleoclimate Archives. In: Stocker, T., Qin, D., Plattner, G., Tignor, M., Allen, S., Boschung, J., Nauels, A., Xia, Y., Bex, V., Midgley, P. (Eds.), Working Group I Contribution to the Fifth Assessment Report of the Intergovernmental Panel on Climate Change. Cambridge University Press, Cambridge, United Kingdom and New York, NY, USA.

Menounos, B., 1997. The water content of lake sediments and its relationship to other physical parameters: an alpine case study. Holocene 7, 207–212.

Müller, J., Werner, K., Stein, R., Fahl, K., Moros, M., Jansen, E., 2012. Holocene cooling culminates in sea ice oscillations in Fram Strait. Quat. Sci. Rev. 47, 1–14.

Mäusbucher, R., Borg, K.v.d, Daug, G., Kroemer, E., Müller, J., Wallner, J., 2002. Late Pleistocene and Holocene environmental changes in NW Spitsbergen – evidence from lake sediments. Z. Geomorphol. 46, 417–439.

Nesje, A., 1992. A piston corer for lacustrine and marine sediments. Arct. Alp. Res. 24, 257–259.

Nesje, A., Dahl, S.O., Anderson, C., Matthews, J.A., 2000. The lacustrine sedimentary sequence in Sygneskardvatnet, western Norway: a continous, high-resolution record of the Jostedalsbreen ice cap during the Holocene. Quat. Sci. Rev. 19, 1047–1065.

Nesje, A., Kvamme, M., Rye, N., Løvlie, R., 1991. Holocene glacial and climate history of the Jostedalsbreen region, Western Norway; evidence from lake sediments and terrestrial deposits. Quat. Sci. Rev. 10, 87–114.

Oerlemans, J., 2005. Extracting a climate signal from 169 glacier records. Science 308, 675–677.

Ohta, Y., Piepjohn, K., Dallmann, W.K., Elvevold, S., 2008. Geological Map of Svalbard 1:100,000, Sheet A6G Krossfjorden. In: Temakart No. 42. Norsk Polarinstitutt.

Osmaston, H., 2005. Estimates of glacier equilibrium line altitudes by the Area×Altitude, the Area× Altitude Balance Ratio and the Area× Altitude Balance Index methods and their validation. Quat. Int. 138, 22–31.

Paasche, Ø., Larsen, J., 2010. Changes in lake stratification and oxygen distribution inferred from two contrasting records of magnetotactic bacteria and diatoms. J. Geophys. Res. Biogeosci. 115, G02012.

Paasche, Ø., Løvlie, R., 2011. Synchronized postglacial colonization by magnetotactic bacteria. Geology 39, 75–78.

Paasche, Ø., Løvlie, R., Dahl, S.O., Bakke, J., Nesje, A., 2004. Bacterial magnetite in lake sediments: late glacial to Holocene climate and sedimentary changes in northern Norway. Earth Planet. Sci. Lett. 223, 319–333.

Porter, S.C., 1975. Equilibrium-line altitudes of late Quaternary glaciers in the Southern Alps, New Zealand. Quat. Res. 5, 27–47.

Rea, B.R., 2009. Defining modern day Area-Altitude Balance Ratios (AABRs) and their use in glacier-climate reconstructions. Quat. Sci. Rev. 28, 237–248.

Reimer, P.J., Bard, E., Bayliss, A., Beck, J.W., Blackwell, P.G., Ramsey, C.B., Grootes, P.M., Guilderson, T.P., Haflidason, H., Hajdas, I., 2013. IntCal13 and Marine13 radiocarbon age calibration curves 0–50,000 years cal BP. Radiocarbon 55, 1869–1887.

Reusche, M., Winsor, K., Carlson, A.E., Marcott, S.A., Rood, D.H., Novak, A., Roof, S., Retelle, M., Werner, A., Caffee, M., Clark, P.U., 2014. 10Be surface exposure ages on the late-Pleistocene and Holocene history of Linnébreen on Svalbard. Quat. Sci. Rev. 89, 5–12.

Rubensdotter, L., Rosqvist, G., 2009. Influence of geomorphological setting, fluvial-, glaciofluvial- and mass-movement processes on sedimentation in alpine lakes. Holocene 19, 665–678.

Ruff, M., Wacker, L., Gggeler, H., Synal, H., Szidat, S., 2007. A gas ion source for radiocarbon measurements at 200 kV. Radiocarbon 49, 307–314.

Salvigsen, O., 1979. The last deglaciation of Svalbard. Boreas 7, 229–251.

Salvigsen, O., 2002. Radiocarbon-dated *Mytilus edulis* and Modiolus modiolus from northern Svalbard: climatic implications. Nor. Geogr. Tidsskr. 56, 56–61.

Salvigsen, O., Forman, S.L., Miller, G.H., 1992. Thermophilous molluscs on Svalbard during the Holocene and their paleoclimatic implications. Polar Res. 11, 1–10.

Sarnthein, M., Van Kreveld, S., Erlenkeuser, H., Grootes, P.M., Kucera, M., Pflaumann, U., Schulz, M., 2003. Centennial-to-millennial-scale periodicities of Holocene climate and sediment injections off the western Barents shelf, 75°N. Boreas 32, 447–461.

Schomacker, A., Kjær, K.H., 2007. Origin and de-icing of multiple generations of ice-cored moraines at Brúarjökull, Iceland. Boreas 36, 411–425.

Snyder, J.A., Miller, G.H., Werner, A., Jull, A.J.T., Stafford, T.W., 1994. AMS-radiocarbon dating of organic-poor lake sediment, an example from Linnévatnet, Spitsbergen, Svalbard. Holocene 4, 413–421.

Snyder, J.A., Werner, A., Miller, G.H., 2000. Holocene cirque glacier activity in western Spitsbergen, Svalbard: sediment records from proglacial Linnévatnet. Holocene 10, 555–563.

Steinhilber, F., Beer, J., Fröhlich, C., 2009. Total solar irradiance during the Holocene. Geophys. Res. Lett. 36, L19704.

Stolz, J.F., Lovley, D.R., Haggerty, S.E., 1990. Biogenic magnetite and the magnetization of sediments. J. Geophys. Res. Solid Earth 95, 4355–4361.

Sund, M., Lauknes, T.R., Eiken, T., 2014. Surge dynamics in the Nathorstbreen glacier system, Svalbard. Cryosphere 8, 623–638.

Svendsen, J.I., Mangerud, J., 1997. Holocene glacial and climatic variations on Spitsbergen, Svalbard. Holocene 7, 45–57.

Svendsen, J.I., Mangerud, J., Miller, G.H., 1989. Denudation rates in the Arctic estimated from lake sediments on Spitsbergen, Svalbard. Palaeogeogr. Palaeoclimatol. Palaeoecol. 76, 153–168.

Syms, C., 2008. Principle components analysis. In: Jørgensen, S.E., Fath, B.D. (Eds.), Encyclopedia of Ecology. Academic Press, Oxford, pp. 2940–2949.

Vasskog, K., Paasche, Ø., Nesje, A., Boyle, J.F., Birks, H.J.B., 2012. A new approach for reconstructing glacier variability based on lake sediments recording input from more than one glacier. Quat. Res. 77, 192–204.

Vinther, B.M., Clausen, H.B., Fisher, D.A., Koerner, R.M., Johnsen, S.J., Andersen, K.K., Dahl-Jensen, D., Rasmussen, S.O., Steffensen, J.P., Svensson, A.M., 2008. Synchronizing ice cores from the Renland and Agassiz ice caps to the Greenland Ice Core Chronology. J. Geophys. Res. Atmos. 113, D08115.

Wanner, H., Beer, J., Bütikofer, J., Crowley, T.J., Cubasch, U., Flückiger, J., Goosse, H., Grosjean, M., Joos, F., Kaplan, J.O., Küttel, M., Müller, S.A., Prentice, I.C., Solomina, O., Stocker, T.F., Tarasov, P., Wagner, M., Widmann, M., 2008. Mid- to Late Holocene climate change: an overview. Quat. Sci. Rev. 27, 1791–1828.

Werner, A., 1993. Holocene moraine chronology, Spitsbergen, Svalbard: lichenometric evidence for multiple neoglacial advances in the Arctic. Holocene 3, 128–137.